2

MAGNETIC STRUCTURES

The *mean-field theory* introduced in the previous section is used in this chapter as a basis for examining some of the magnetic structures assumed by the rare earth metals. The theory is presented at length in the first section. Beginning with the expression for the free energy, some general results are established for the magnetization, and applied analytically to the calculation of the susceptibility in the *high-temperature* limit. The mean-field approximation is then developed, and a numerical method for solving the resulting equations self-consistently, for magnetic structures which are commensurable with the lattice, is described. The *Landau expansion* of the free energy in terms of the *order parameters* of the magnetic system provides the starting point for a discussion of a number of the periodic magnetic structures which arise as a result of the long range of the indirect-exchange interaction. The ordering temperatures are calculated by analytical means, and the relative stability of different structures compared. In the following section, the important extension by Callen and Callen of the Zener power-law for the temperature dependence of the magnetic anisotropy is derived. The thermal expectation values $\langle O_l^m \rangle$ of the *Stevens operators* are calculated and their dependence on the magnetization determined. From the free energy, the *magnetic anisotropy* and the *magnetoelastic coefficients* are deduced. We conclude with a detailed discussion of some *magnetic structures*, using the aforementioned analytical methods, supplemented by numerical calculations, to help identify those characteristics of the magnetic interactions which lead to the stability of different moment-configurations under various conditions. This account is illustrated by various examples, with emphasis on the the diverse magnetic phases of Ho. Among other structures, we consider the *ferromagnet*, the *cone*, the *helix*, the *longitudinal wave*, the *cycloid*, and commensurable *spin slips*. The effect of a magnetic field in stabilizing *fan* and *helifan* structures, and the ordering of *thin films* and *superlattices*, are also discussed.

2.1 Mean-field theory of magnetic ordering

The simplest form of Hamiltonian which is adequate to explain the occurrence of most of the observed magnetic structures is

$$\mathcal{H} = \sum_i \mathcal{H}_{\rm cf}(i) - \frac{1}{2}\sum_{ij} \mathcal{J}(ij)\,\mathbf{J}_i \cdot \mathbf{J}_j + \mathcal{H}_{\rm Z}, \qquad (2.1.1a)$$

where the first sum is the single-ion crystal-field Hamiltonian

$$\mathcal{H}_{\rm cf}(i) = \sum_{l=2,4,6} B_l^0 O_l^0(\mathbf{J}_i) + B_6^6 O_6^6(\mathbf{J}_i), \tag{2.1.1b}$$

the two-ion term is assumed to be isotropic, and the Zeeman term is

$$\mathcal{H}_{\rm Z} = -\sum_i \boldsymbol{\mu}_i \cdot \mathbf{H}_i. \tag{2.1.1c}$$

The field may vary spatially, so that we must specify its value on each site, writing $\mathbf{H}_i \equiv \mathbf{H}(\mathbf{R}_i)$, and the magnetic moment on the ith ion is $\boldsymbol{\mu}_i = g\mu_B \mathbf{J}_i$.

The static-susceptibility tensor may be derived as the second derivative of the free energy, and we shall therefore begin by recapitulating a few basic thermodynamic results. The free energy is

$$F = U - TS = -\frac{1}{\beta} \ln Z, \tag{2.1.2}$$

where U is the internal energy, S the entropy, and $\beta = (k_B T)^{-1}$. The partition function is

$$Z = \mathrm{Tr}\{e^{-\beta\mathcal{H}}\} = \sum_p e^{-\beta E_p}. \tag{2.1.3}$$

Tr indicates the trace over a complete set of states, and the final summation may be performed if the eigenvalues E_p of the Hamiltonian are known. The expectation value of an operator A is

$$\langle A \rangle = \frac{1}{Z} \mathrm{Tr}\{A e^{-\beta\mathcal{H}}\}. \tag{2.1.4}$$

The derivative of the free energy with respect to a variable x is

$$\frac{\partial F}{\partial x} = -\frac{1}{\beta Z}\frac{\partial Z}{\partial x} = \frac{1}{Z}\mathrm{Tr}\left\{\frac{\partial \mathcal{H}}{\partial x} e^{-\beta\mathcal{H}}\right\} = \left\langle \frac{\partial \mathcal{H}}{\partial x} \right\rangle. \tag{2.1.5}$$

This expression is obtained by utilizing the invariance of the trace to the basis used, assuming it to be independent of x and a cyclic permutation of the operators, thus allowing a conventional differentiation of the exponential operator, as may be seen by a Taylor expansion. This result is general, but the exponential operator can only be treated in this simple way in second derivatives if $\partial\mathcal{H}/\partial x$ commutes with the Hamiltonian, which is usually not the case. However, we may be interested only in the leading-order contributions in the limit where β is small, i.e. at *high*

temperatures. Expanding in powers of β, we may use the approximation $\exp\{-\beta\mathcal{H}\} \simeq 1 - \beta\mathcal{H} + \frac{1}{2}\beta^2\mathcal{H}^2$. In this case, we may proceed as above, and the result is

$$\begin{aligned}\frac{\partial^2 F}{\partial x \partial y} = \Big\langle \frac{\partial^2 \mathcal{H}}{\partial x \partial y} \Big\rangle + \beta\Big(\Big\langle \frac{\partial \mathcal{H}}{\partial x} \Big\rangle \Big\langle \frac{\partial \mathcal{H}}{\partial y} \Big\rangle - \Big\langle \frac{\partial \mathcal{H}}{\partial x} \frac{\partial \mathcal{H}}{\partial y} \Big\rangle \Big) \\ - \frac{\beta^2}{2} \Big\langle \Big[\frac{\partial \mathcal{H}}{\partial x} \,,\, \frac{\partial \mathcal{H}}{\partial y} \Big] \mathcal{H} \Big\rangle + \mathcal{O}(\beta^3),\end{aligned} \tag{2.1.6}$$

where the second- and higher-order terms vanish if one of the derivatives of $\mathcal{H}$ commutes with $\mathcal{H}$ itself.

In many instances, it is more convenient to consider the angular momentum rather than the magnetic moment, with a corresponding field variable $\mathbf{h}_i = g\mu_B \mathbf{H}_i$, so that the Zeeman term (2.1.1*c*) becomes

$$\mathcal{H}_{\rm Z} = -\sum_i \boldsymbol{\mu}_i \cdot \mathbf{H}_i = -\sum_i \mathbf{J}_i \cdot \mathbf{h}_i. \tag{2.1.7}$$

Since the exchange and anisotropy terms in $\mathcal{H}$ do not depend explicitly on the field, $\partial\mathcal{H}/\partial H_{i\alpha} = -\mu_{i\alpha}$ and, using eqn (2.1.5), we have

$$\langle \mu_{i\alpha} \rangle = -\partial F/\partial H_{i\alpha} \quad \text{or} \quad \langle J_{i\alpha} \rangle = -\partial F/\partial h_{i\alpha}. \tag{2.1.8}$$

Next, we define the non-local susceptibilities

$$\chi^{\mu}_{\alpha\beta}(ij) = \partial\langle \mu_i \rangle / \partial H_{j\beta} = -\partial^2 F/\partial H_{i\alpha}\partial H_{j\beta}, \tag{2.1.9a}$$

and similarly

$$\chi^{\mathbf{J}}_{\alpha\beta}(ij) = (g\mu_B)^{-2}\chi^{\mu}_{\alpha\beta}(ij) = -\partial^2 F/\partial h_{i\alpha}\partial h_{j\beta}, \tag{2.1.9b}$$

and the corresponding Fourier transforms, e.g.

$$\chi^{\mathbf{J}}_{\alpha\beta}(\mathbf{q}) = \frac{1}{N}\sum_{ij} \chi^{\mathbf{J}}_{\alpha\beta}(ij) e^{-i\mathbf{q}\cdot(\mathbf{R}_i - \mathbf{R}_j)} = \sum_j \chi^{\mathbf{J}}_{\alpha\beta}(ij) e^{-i\mathbf{q}\cdot(\mathbf{R}_i - \mathbf{R}_j)}. \tag{2.1.9c}$$

The final equality only applies in a uniform system. If the field is increased by an infinitesimal amount $\delta\mathbf{H}(\mathbf{q})\exp(i\mathbf{q}\cdot\mathbf{R}_i)$, the individual moments are changed by

$$\delta\langle \mu_{i\alpha} \rangle = \sum_j \sum_\beta \chi^{\mu}_{\alpha\beta}(ij)\delta H_\beta(\mathbf{q}) e^{i\mathbf{q}\cdot\mathbf{R}_j}, \tag{2.1.10a}$$

according to (2.1.9). Hence the added harmonically-varying field introduces one Fourier component in the magnetization:

$$\delta M_\alpha(\mathbf{q}) = \frac{1}{V}\sum_i \delta\langle \mu_{i\alpha} \rangle e^{-i\mathbf{q}\cdot\mathbf{R}_i} = \frac{N}{V}\sum_\beta \chi^{\mu}_{\alpha\beta}(\mathbf{q})\delta H_\beta(\mathbf{q}), \tag{2.1.10b}$$

proportional to the susceptibility at the wave-vector considered. The usual definition of the susceptibility components (per unit volume), as used in Chapter 1, is $\delta M_\alpha(\mathbf{q})/\delta H_\beta(\mathbf{q})$. The susceptibility used in (2.1.10*b*) differs from this by the factor V/N, i.e. we are here considering the susceptibility per atom instead of per unit volume. Furthermore, since we shall not make any further use of $\chi^{\mu}_{\alpha\beta}(\mathbf{q})$, we shall reserve the notation $\chi_{\alpha\beta}(\mathbf{q})$ for the $\mathbf{q}$-dependent susceptibility $\chi^{\mathbf{J}}_{\alpha\beta}(\mathbf{q})$, introduced in eqn (2.1.9*b*), throughout the rest of the book. So in terms of the susceptibility per atom, 'in units of $(g\mu_B)^2$', the above equation may be written

$$\delta\langle J_\alpha(\mathbf{q})\rangle = \frac{1}{N}\sum_i \delta\langle J_{i\alpha}\rangle e^{-i\mathbf{q}\cdot\mathbf{R}_i} = \sum_\beta \chi_{\alpha\beta}(\mathbf{q})\delta h_\beta(\mathbf{q}), \qquad (2.1.10c)$$

with the upper index $\mathbf{J}$ in $\chi^{\mathbf{J}}_{\alpha\beta}(\mathbf{q})$ being suppressed from now on.

2.1.1 The high-temperature susceptibility

In order to calculate $\overline{\overline{\chi}}(\mathbf{q})$ in zero field, we shall first use the approximation (2.1.6) to the derivative of the free energy, valid at high temperatures. In this limit $\langle \mathbf{J}_i\rangle = \mathbf{0}$, and only one term in the expansion is non-zero:

$$\chi_{\alpha\beta}(ij) = \beta \mathrm{Tr}\{J_{i\alpha}J_{j\beta}(1-\beta\mathcal{H})\}/\mathrm{Tr}\{1-\beta\mathcal{H}\}, \qquad (2.1.11)$$

to second order in β. The commutator in the third term on the right-hand side of (2.1.6) is either zero or purely imaginary (if $i = j$ and $\alpha \neq \beta$), showing immediately that the expectation value of this term must vanish in all cases. To first order in β, we obtain from (2.1.11)

$$\chi_{\alpha\beta}(ij) \simeq \beta \mathrm{Tr}\{J_{i\alpha}J_{j\beta}\}/\mathrm{Tr}\{1\} = \tfrac{1}{3}J(J+1)\beta\delta_{\alpha\beta}\delta_{ij}\,,$$

using the product of the eigenvectors of $J_{i\alpha}$ as the basis, and recalling that

$$\sum m^2 = \tfrac{1}{3}J(J+1)(2J+1),$$

when m runs from $-J$ to J. In order to calculate the second-order contribution, we shall utilize the general tensor properties of the Stevens operators, which satisfy the orthogonality condition:

$$\begin{aligned} &\mathrm{Tr}\{O_l^m(\mathbf{J}_i)O_{l'}^{m'}(\mathbf{J}_j)\} = \delta_{ij}\delta_{ll'}\delta_{mm'}\mathrm{Tr}\{[O_l^m(\mathbf{J}_i)]^2\} \\ \text{and} \quad &\mathrm{Tr}\{O_l^m(\mathbf{J}_i)\} = 0, \end{aligned} \qquad (2.1.12)$$

when l and l' are both non-zero. O_0^0 is just the identity operator. $J_{i\alpha}$ is a linear combination of $O_1^m(\mathbf{J}_i)$, $m = -1, 0, 1$, and (2.1.12) then implies

that the trace of the Hamiltonian (2.1.1) vanishes, and hence that the denominator in (2.1.11) is $\mathrm{Tr}\{1\} = (2J+1)^N$. For the second-order term in the numerator, we find

$$\begin{aligned}\mathrm{Tr}\big\{J_{i\alpha}J_{j\beta}\mathcal{H}\big\} &= \delta_{ij}B_2^0\mathrm{Tr}\big\{J_{i\alpha}J_{i\beta}O_2^0(\mathbf{J}_i)\big\} - \mathcal{J}(ij)\mathrm{Tr}\big\{J_{i\alpha}J_{j\beta}\mathbf{J}_i\cdot\mathbf{J}_j\big\}\\ &= \delta_{ij}\delta_{\alpha\beta}B_2^0\mathrm{Tr}\big\{J_{i\alpha}^2[3J_{iz}^2 - J(J+1)]\big\} - \delta_{\alpha\beta}\mathcal{J}(ij)\mathrm{Tr}\big\{J_{i\alpha}^2J_{j\alpha}^2\big\},\end{aligned}$$

utilizing that $J_{i\alpha}J_{j\beta}$ is a linear combination of second- and lower-rank tensors for $i = j$, and a product of first-rank tensors for $i \neq j$. When $\alpha = z$ (or ζ), we may readily calculate the first trace, using

$$\sum m^4 = \tfrac{1}{15}J(J+1)(2J+1)(3J^2+3J-1).$$

The traces with $\alpha = x$ or $\alpha = y$ must be equal, and using this equality in the case $\alpha = x$, for instance, we may replace J_x^2 in the trace by $\frac{1}{2}(J_x^2 + J_y^2) \to \frac{1}{2}J(J+1) - \frac{1}{2}J_z^2$. As the constant term multiplied by $3J_z^2 - J(J+1)$ does not contribute (as $\mathrm{Tr}\{3J_z^2 - J(J+1)\} = 0$), the trace with $\alpha = x$ or y is equal to $-1/2$ times that with $\alpha = z$. Only the single-ion terms contribute to the trace when $i = j$ ($\mathcal{J}(ii)$ is assumed to be zero), and of these only the lowest-rank term B_2^0 appears, to leading order. The two-ion coupling only occurs in the trace, and hence in $\chi_{\alpha\beta}(ij)$, when $i \neq j$, and this contribution may be straightforwardly calculated. To second order in β, the off-diagonal terms are zero, whereas

$$\begin{aligned}\chi_{\alpha\alpha}(ij) = \delta_{ij}\tfrac{1}{3}J(J+1)\beta\big[1 - \tfrac{2}{5}(3\delta_{\alpha\zeta}-1)B_2^0(J-\tfrac{1}{2})(J+\tfrac{3}{2})\beta\big]\\ + \big[\tfrac{1}{3}J(J+1)\beta\big]^2\mathcal{J}(ij).\end{aligned}$$

Introducing the Fourier transform of the two-ion coupling,

$$\mathcal{J}(\mathbf{q}) = \sum_j \mathcal{J}(ij)e^{-i\mathbf{q}\cdot(\mathbf{R}_i - \mathbf{R}_j)}, \tag{2.1.13}$$

we find that, to the order considered, the inverse of the **q**-dependent susceptibility may be written

$$1/\chi_{\alpha\alpha}(\mathbf{q}) = \frac{3k_BT}{J(J+1)} + (3\delta_{\alpha\zeta}-1)\frac{6(J-\frac{1}{2})(J+\frac{3}{2})}{5J(J+1)}B_2^0 - \mathcal{J}(\mathbf{q}) + \mathcal{O}(1/T). \tag{2.1.14}$$

The inverse susceptibility in the high-temperature limit thus increases linearly with the temperature, with a slope inversely proportional to the square of the effective paramagnetic moment ($\propto \{J(J+1)\}^{1/2}$). The susceptibilities determined experimentally by magnetization measure-

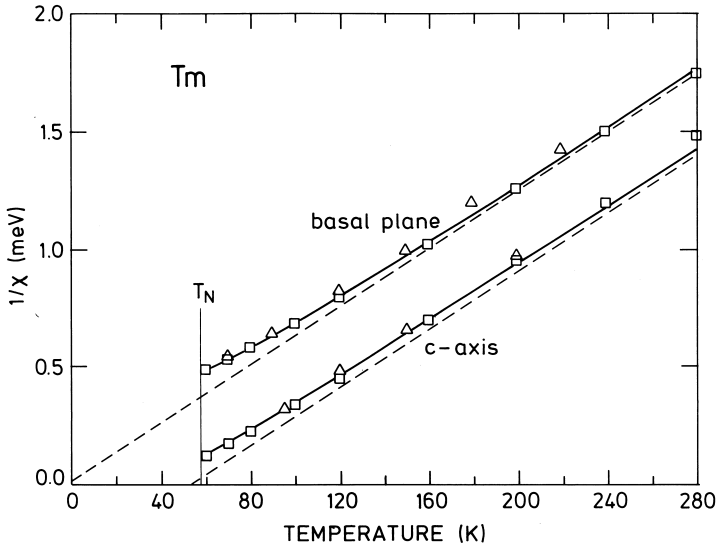

Fig. 2.1. The inverse susceptibility, in atomic units, in Tm above T_N. The full lines depict the results of a mean-field calculation and the dashed lines are extrapolations of the high-temperature limit. Experimental values are also shown. The MF theory predicts a deviation from the high-temperature expression as the ordering temperature is approached from above, because of crystal-field anisotropy effects.

ments are the bulk values at zero wave-vector. The straight lines found at high temperatures for the inverse-susceptibility components $1/\chi_{\alpha\alpha}(\mathbf{0})$ versus temperature may be extrapolated to lower values, as illustrated in Fig. 2.1. The values at which these lines cross the temperature axis are the *paramagnetic Curie temperatures* $\theta_\parallel$ and $\theta_\perp$, determined respectively when the field is parallel and perpendicular to the c-axis (ζ-axis). The high-temperature expansion then predicts these temperatures to be

$$k_B\theta_\parallel = \tfrac{1}{3}J(J+1)\mathcal{J}(\mathbf{0}) - \tfrac{4}{5}(J-\tfrac{1}{2})(J+\tfrac{3}{2})B_2^0, \qquad (2.1.15a)$$

and

$$k_B\theta_\perp = \tfrac{1}{3}J(J+1)\mathcal{J}(\mathbf{0}) + \tfrac{2}{5}(J-\tfrac{1}{2})(J+\tfrac{3}{2})B_2^0. \qquad (2.1.15b)$$

Hence the paramagnetic Curie temperatures are determined by the lowest-rank interactions in the Hamiltonian, i.e. those terms for which $l+l'=2$. The difference between the two temperatures depends only on B_2^0, because of the assumption that the two-ion coupling is an *isotropic*

Heisenberg exchange. The mean temperature $(\theta_{\parallel}+2\theta_{\perp})/3$ is determined by $\mathcal{J}(\mathbf{0})$ which, from (2.1.13), is the algebraic sum of the isotropic two-ion interactions, and this temperature may be measured directly with a polycrystalline sample. The two basal-plane components are found to be equal. This is not just due to the assumption of high temperatures, but is generally valid as long as there is no ordered moment in the basal-plane. In this case, the c-axis is a three-fold symmetry axis, or effectively a six-fold axis, due to the symmetry of the basal-plane anisotropy B_6^6 in the Hamiltonian. The susceptibility is a second-rank tensor, according to (2.1.9), and it cannot therefore vary under rotation about a three- or six-fold axis.

2.1.2 The mean-field approximation

The high-temperature expansion may be extended to higher order in β, but the calculations rapidly become more complex, so we shall instead adopt another approach, the mean-field approximation. In this method, the correlated fluctuations of the moments around their equilibrium values are neglected. In order to introduce $\langle\mathbf{J}_i\rangle$ into the Hamiltonian, we utilize the identity

$$\mathbf{J}_i\cdot\mathbf{J}_j=(\mathbf{J}_i-\langle\mathbf{J}_i\rangle)\cdot(\mathbf{J}_j-\langle\mathbf{J}_j\rangle)+\mathbf{J}_i\cdot\langle\mathbf{J}_j\rangle+\mathbf{J}_j\cdot\langle\mathbf{J}_i\rangle-\langle\mathbf{J}_i\rangle\cdot\langle\mathbf{J}_j\rangle.$$

The MF approximation then consists in neglecting the first term on the right-hand side, which is associated with two-site fluctuations, since $i\neq j$. The Hamiltonian (2.1.1) is then effectively decoupled into a sum of N independent terms for the single sites; $\mathcal{H}\simeq\sum_i\mathcal{H}_{\rm MF}(i)$, where

$$\mathcal{H}_{\rm MF}(i)=\mathcal{H}_{\rm cf}(i)-\mathbf{J}_i\cdot\mathbf{h}_i-\big(\mathbf{J}_i-\tfrac{1}{2}\langle\mathbf{J}_i\rangle\big)\cdot\sum_j\mathcal{J}(ij)\langle\mathbf{J}_j\rangle,\qquad(2.1.16)$$

in the presence of an external magnetic field $\mathbf{h}_i=g\mu_B\mathbf{H}_i$. Introducing the effective field

$$\mathbf{h}_i^{\rm eff}=\mathbf{h}_i+\sum_j\mathcal{J}(ij)\langle\mathbf{J}_j\rangle,\qquad(2.1.17a)$$

we may write the MF Hamiltonian

$$\mathcal{H}_{\rm MF}(i)=\mathcal{H}_{\rm cf}(i)-\mathbf{J}_i\cdot\mathbf{h}_i^{\rm eff}+\tfrac{1}{2}\langle\mathbf{J}_i\rangle\cdot(\mathbf{h}_i^{\rm eff}-\mathbf{h}_i).\qquad(2.1.17b)$$

Self-consistent solutions of the MF equations may sometimes be obtained analytically, but numerical methods may be used more generally, provided that the periodicity of the magnetic structure is commensurable with that of the lattice. For an assumed distribution of $\langle\mathbf{J}_j\rangle$, the effective field and hence the MF Hamiltonian for the ith site is calculated.

Diagonalizing this Hamiltonian, we may derive the partition function Z_i, the free energy F_i, and the expectation value $\langle \mathbf{J}_i \rangle$ for this site. The last term in (2.1.17*b*) just adds a constant contribution to F_i, without affecting $\langle \mathbf{J}_i \rangle$. Performing this calculation for all the different ions, we determine the various values of $\langle \mathbf{J}_j \rangle$, and the total free energy is the sum of the F_i. The derived values of $\langle \mathbf{J}_j \rangle$ are used as the input for a new MF Hamiltonian, and this iterative procedure is repeated until self-consistency is attained. The self-consistent solution of the MF Hamiltonian may be one in which $\langle \mathbf{J}_i \rangle$ is non-zero even in zero field, thus describing the occurrence of a spontaneous ordering of the moments.

Having found the self-consistent solution for the angular momenta, we may proceed to calculate the susceptibility. The MF Hamiltonian for the ith site has been diagonalized, and we shall denote the $(2J+1)$ eigenstates by $|\, p >$, with corresponding energy eigenvalues E_p. If the effective field is changed by a small amount $\delta h_\beta^{\text{eff}}$, the Zeeman term $-J_{i\beta}\delta h_\beta^{\text{eff}}$ must be added to the Hamiltonian, and $E_p^{(1)} = E_p - < p \,|\, J_{i\beta} \,|\, p > \delta h_\beta^{\text{eff}}$, to first order in the perturbation, provided that $|\, p >$ is a set which diagonalizes the perturbation within the possibly degenerate subspaces of the zero-field Hamiltonian. The new eigenstates are

$$|\, p^{(1)} > = |\, p > - \delta h_\beta^{\text{eff}} {\sum_{p'}}' |\, p' >< p' \,|\, J_{i\beta} \,|\, p > /(E_p - E_{p'}),$$

where the terms for which $E_p = E_{p'}$ vanish. Using (2.1.3) and (2.1.4), we then have, to first order in $\delta h_\beta^{\text{eff}}$,

$$\begin{aligned} \langle J_{i\alpha}^{(1)} \rangle = \sum_p < p^{(1)} \,|\, J_{i\alpha} \,|\, p^{(1)} > n_p^{(1)} &= \sum_p < p \,|\, J_{i\alpha} \,|\, p > n_p^{(1)} \\ &- \delta h_\beta^{\text{eff}} {\sum_{pp'}}' < p \,|\, J_{i\alpha} \,|\, p' >< p' \,|\, J_{i\beta} \,|\, p > n_p/(E_p - E_{p'}) \\ &- \delta h_\beta^{\text{eff}} {\sum_{pp'}}' < p \,|\, J_{i\beta} \,|\, p' >< p' \,|\, J_{i\alpha} \,|\, p > n_p/(E_p - E_{p'}), \end{aligned}$$

where the last two sums extend over states for which $E_p \neq E_{p'}$. The population factor of the pth level at $\delta h_\beta^{\text{eff}} = 0$ is $n_p = \exp(-\beta E_p)/Z_i$, and $n_p^{(1)}$ is the corresponding factor at the field $\delta h_\beta^{\text{eff}}$. By differentiation, we find

$$\begin{aligned} \partial n_p^{(1)} / \partial (\delta h_\beta^{\text{eff}}) &= \Big\{ < p \,|\, J_{i\beta} \,|\, p > - \sum_{p'} < p' \,|\, J_{i\beta} \,|\, p' > n_{p'} \Big\} \beta n_p \\ &= \big\{ < p \,|\, J_{i\beta} \,|\, p > - \langle J_{i\beta} \rangle \big\} \beta n_p. \end{aligned}$$

Introducing this result in the equation above, and interchanging p and

p' in the last sum, we obtain finally:

$$\chi^o_{\alpha\beta}(i) = \partial\langle J_{i\alpha}\rangle/\partial h^{\rm eff}_\beta = \sum_{pp'}^{E_p\neq E_{p'}} \frac{<p\,|\,J_{i\alpha}\,|\,p'><p'\,|\,J_{i\beta}\,|\,p>}{E_{p'}-E_p}(n_p - n_{p'})$$
$$+\ \beta \sum_{pp'}^{E_p=E_{p'}} <p\,|\,J_{i\alpha}\,|\,p'><p'\,|\,J_{i\beta}\,|\,p>\, n_p - \beta\langle J_{i\alpha}\rangle\langle J_{i\beta}\rangle. \quad (2.1.18)$$

The second summation is transformed in such a way that it is no longer necessary for $J_{i\beta}$ to be diagonal within the degenerate subspaces, as required initially. The first term in the susceptibility is the *Van Vleck* contribution, which becomes constant at zero temperature, whereas the second term, the *Curie* contribution, diverges as $1/T$ in the low-temperature limit. The susceptibility deduced above is that determining the response due to a change of the *effective* field, $\delta\langle\mathbf{J}_i\rangle = \overline{\overline{\chi}}^{\,o}(i)\delta\mathbf{h}^{\rm eff}_i$, whereas we wish to know the response due to a small change of the *external* field. If a small harmonically-varying field $\delta\mathbf{h}_\mathbf{q}\exp(i\mathbf{q}\cdot\mathbf{R}_i)$ is applied, the effective field, according to (2.1.17a), is

$$\delta\mathbf{h}^{\rm eff}_i = \delta\mathbf{h}_\mathbf{q} e^{i\mathbf{q}\cdot\mathbf{R}_i} + \sum_j \mathcal{J}(ij)\overline{\overline{\chi}}^{\,o}(j)\delta\mathbf{h}^{\rm eff}_j.$$

This equation may be solved by a Fourier transformation if $\overline{\overline{\chi}}^{\,o}(i) = \overline{\overline{\chi}}^{\,o}$ is site-independent, which it is so long as $\langle\mathbf{J}_i\rangle$ is independent of i, as in the high-temperature paramagnetic phase, for example, where $\langle\mathbf{J}_i\rangle = \mathbf{0}$. Neglecting any site-dependence of $\overline{\overline{\chi}}^{\,o}$, and introducing the notation $\delta\mathbf{h}^{\rm eff}_i = \delta\mathbf{h}^{\rm eff}_\mathbf{q}\exp(i\mathbf{q}\cdot\mathbf{r}_i)$, we get

$$\delta\mathbf{h}^{\rm eff}_\mathbf{q} = \left\{1 - \overline{\overline{\chi}}^{\,o}\mathcal{J}(\mathbf{q})\right\}^{-1}\delta\mathbf{h}_\mathbf{q},$$

or, by the definition of the susceptibility,

$$\overline{\overline{\chi}}(\mathbf{q}) = \left\{1 - \overline{\overline{\chi}}^{\,o}\mathcal{J}(\mathbf{q})\right\}^{-1}\overline{\overline{\chi}}^{\,o}. \quad (2.1.19a)$$

In the following, we shall assume that the external magnetic field is zero. With this restriction, $\overline{\overline{\chi}}(\mathbf{q})$ is diagonal in the $(\xi\eta\zeta)$-coordinate system, and the reciprocal susceptibility, in the MF approximation, may be written

$$1/\chi_{\alpha\alpha}(\mathbf{q}) = 1/\chi^o_{\alpha\alpha} - \mathcal{J}(\mathbf{q}). \quad (2.1.19b)$$

In the degenerate case, (2.1.18) implies that $\chi^o_{\alpha\alpha} = \beta J(J+1)/3$. However, if $\mathcal{H}_{\rm cf}$ is non-zero, the expression (2.1.18) for the susceptibility becomes quite complex. A drastic simplification is achieved by assuming a

small value of β. In this high temperature limit, $\overline{\overline{\chi}}^{o}$ may be calculated by a procedure equivalent to that used in deriving (2.1.14), except that $\mathcal{J}(ij) = 0$. Hence, to second order in β, we have

$$\chi^{o}_{\alpha\alpha} \simeq \tfrac{1}{3}J(J+1)\beta\big[1 - \tfrac{2}{5}(3\delta_{\alpha\zeta} - 1)(J - \tfrac{1}{2})(J + \tfrac{3}{2})B^0_2\beta\big]. \qquad (2.1.20)$$

Introducing (2.1.20) in (2.1.19), we obtain the same result as previously derived in (2.1.14), demonstrating that the MF approximation is correct in the high-temperature limit. Although the thermal fluctuations increase when the temperature is raised, they also become increasingly uncorrelated. It is the latter effect which is the most pronounced, and the correction to the MF value of the free energy, proportional to the correlation energy of the two-site fluctuations $\mathcal{J}(ij)\{\langle \mathbf{J}_i \cdot \mathbf{J}_j\rangle - \langle \mathbf{J}_i\rangle \cdot \langle \mathbf{J}_j\rangle\}$, decreases with temperature at high temperatures. In the other limit of zero temperature, the correlation effects are much stronger, but the fluctuations themselves are small. We may therefore also expect the MF approximation to be accurate in this limit, and to provide a useful interpolation at intermediate temperatures.

$\overline{\overline{\chi}}^{o}$ increases steadily with decreasing temperature. If the crystal-field ground state is degenerate, the second sum in (2.1.18) is non-zero and $\overline{\overline{\chi}}^{o}$ diverges in the zero-temperature limit. Because of the Kramers degeneracy, the ground state is always at least doubly degenerate if $2J$ is odd. When J is an integer, the ground state may be a singlet, in which case $\overline{\overline{\chi}}^{o}$ saturates at a constant value at zero temperature. Except in this special case, it is always possible to find a temperature where $1/\chi_{\alpha\alpha}(\mathbf{q})$ is zero, corresponding to an infinite $\chi_{\alpha\alpha}(\mathbf{q})$. The largest value of the $\mathbf{q}$-dependent susceptibility is found at the wave-vector $\mathbf{Q}$ at which $\mathcal{J}(\mathbf{q})$ has its maximum. Of the three non-zero components of $\overline{\overline{\chi}}(\mathbf{Q})$, the cc-component is the largest if B^0_2 is negative. If B^0_2 is positive, on the other hand, the two equal basal-plane components are the largest. It is the maximum component of the susceptibility at $\mathbf{q} = \mathbf{Q}$ which first diverges when the system is cooled. This divergence signals that the paramagnetic ground-state becomes unstable against the formation of an ordered state in which the moments are modulated with the wave-vector $\mathbf{Q}$, and point along or perpendicular to the c-direction, depending on whether B^0_2 is respectively negative or positive. Hence, a second-order phase transition takes place at this critical temperature, called the Curie temperature, T_C, or the Néel temperature, T_N, depending on whether $\mathbf{Q} = \mathbf{0}$ or $\mathbf{Q} \neq \mathbf{0}$. Just below T_N, the ordered moment $\langle \mathbf{J}_i\rangle$ is small, and the free energy of the ith ion may be expanded in powers of this moment. In order to establish this expansion, we first consider the Hamiltonian $\mathcal{H}'(i) = \mathcal{H}_{\rm cf}(i) - \mathbf{J}_i \cdot \mathbf{h}$. The corresponding free energy may be written

$$F'_i = F_0/N - \langle \mathbf{J}_i\rangle \cdot \mathbf{h} + \sum_{\alpha} A_\alpha \langle J_{i\alpha}\rangle^2 + \sum_{\alpha\beta} B_{\alpha\beta}\langle J_{i\alpha}\rangle^2\langle J_{i\beta}\rangle^2 + \cdots .$$

Except for the field term, this expansion only includes products of components in which the sum of the exponents is even, because of time-reversal symmetry. Using the equilibrium condition $\partial F_i'/\partial\langle J_{i\alpha}\rangle = 0$, and recalling that $\langle J_{i\alpha}\rangle = \chi^o_{\alpha\alpha}(\sigma=0)h_\alpha$ to leading order, in the zero-field limit, we obtain

$$A_\alpha = \left\{2\chi^o_{\alpha\alpha}(\sigma=0)\right\}^{-1}, \tag{2.1.21a}$$

where $\chi^o_{\alpha\alpha}(\sigma=0)$ is the MF susceptibility (2.1.18), in the limit of zero magnetization (field). The susceptibility decreases with increasing magnetization (or field), as described by the fourth-order terms. An order-of-magnitude estimate of $B_{\alpha\beta}$ may be obtained by neglecting $\mathcal{H}_{\rm cf}(i)$. In this case, the magnetization as a function of the field is given by the Brillouin function (1.2.31):

$$\langle J_{i\alpha}\rangle = JB_J(\beta J h_\alpha) \simeq \tfrac{1}{3}J(J+1)\beta h_\alpha\left\{1-\tfrac{1}{15}(J^2+J+\tfrac{1}{2})\beta^2 h_\alpha^2\right\},$$

which, in combination with the equilibrium condition for the free energy, determines $B_{\alpha\alpha}$. The off-diagonal terms may be obtained straightforwardly by utilizing the condition that, when $\mathcal{H}_{\rm cf}(i)$ is neglected, the free energy should be invariant with respect to any rotation of the magnetization vector, implying that all the coefficients $B_{\alpha\beta}$ are equal, or

$$B_{\alpha\beta} \approx \frac{9}{20}\frac{J^2+J+\frac{1}{2}}{J^3(J+1)^3}k_B T. \tag{2.1.21b}$$

The introduction of the crystal-field terms of course modifies this result, but rather little in the high-temperature limit. Under all circumstances, the effective six-fold symmetry around the c-axis implies that $B_{\alpha\beta}$ is symmetric, $B_{\xi\xi} = B_{\eta\eta} = B_{\xi\eta}$, and $B_{\xi\zeta} = B_{\eta\zeta}$, and it also eliminates the possibility that any other fourth-order terms may contribute. The expansion of the free energy of the total system, when the external field is zero, is obtained from the expansion of F_i', summed over i, by substituting the *exchange* field $\mathbf{h}_i^{\rm eff} = \sum_j \mathcal{J}(ij)\langle\mathbf{J}_j\rangle$ for $\mathbf{h}$, and adding the 'constant' $\frac{1}{2}\langle\mathbf{J}_i\rangle\cdot\mathbf{h}_i^{\rm eff}$, so that

$$F = F_0 - \frac{1}{2}\sum_{ij}\mathcal{J}(ij)\langle\mathbf{J}_i\rangle\cdot\langle\mathbf{J}_j\rangle + \sum_i\Big[\sum_\alpha A_\alpha\langle J_{i\alpha}\rangle^2 + \sum_{\alpha\beta}B_{\alpha\beta}\langle J_{i\alpha}\rangle^2\langle J_{i\beta}\rangle^2\Big] \tag{2.1.22}$$

to fourth order in the magnetization. This expansion of the free energy in terms of the *order parameter(s)* is called the *Landau expansion*.

Assuming the ordered phase to be described by a single wave-vector, we may write

$$\langle J_{i\alpha}\rangle = J\sigma_\alpha\cos(\mathbf{q}\cdot\mathbf{R}_i + \varphi_\alpha), \tag{2.1.23}$$

where $\sigma_\alpha = \sigma_\alpha(\mathbf{q})$ is the relative magnetization at the wave-vector $\mathbf{q}$. Introducing this into the free-energy expression, and utilizing the condition that $\sum_i \cos(\mathbf{q}' \cdot \mathbf{R}_i + \varphi) = 0$, if $\mathbf{q}'$ is not a reciprocal lattice vector, we find

$$f = (F - F_0)/N = \tfrac{1}{4} J^2 \sum_\alpha \{2A_\alpha - \mathcal{J}(\mathbf{q})\}\sigma_\alpha^2 + \tfrac{1}{8} J^4 \sum_{\alpha\beta} B_{\alpha\beta}\{2 + \cos 2(\varphi_\alpha - \varphi_\beta)\}\sigma_\alpha^2 \sigma_\beta^2, \quad (2.1.24)$$

if $4\mathbf{q}$ is different from a reciprocal lattice vector. The coefficients of the second power are thus $\propto \{2A_\alpha - \mathcal{J}(\mathbf{q})\} = 1/\chi_{\alpha\alpha}(\mathbf{q}, \sigma = 0)$, where the susceptibility is evaluated at zero magnetization. As long as all the second-order coefficients are positive, at any value of $\mathbf{q}$, the free energy is at its minimum when $\sigma_\alpha = 0$, i.e. the system is paramagnetic. The smallest of these coefficients are those at $\mathbf{q} = \mathbf{Q}$, where $\mathcal{J}(\mathbf{q})$ has its maximum. In the heavy rare earths, with the exception of Gd, $\mathbf{Q}$ is non-zero and is directed along the c-axis. Depending on the sign of B_2^0, the magnetic structures occurring in the heavy rare earths may be divided into two classes, which we will discuss in turn.

2.1.3 Transversely ordered phases

When $B_2^0 > 0$, as in Tb, Dy, and Ho, the two basal-plane components of $\overline{\overline{\chi}}(\mathbf{Q})$ both diverge at the same critical temperature T_N. Using the approximate high-temperature value (2.1.20) for the susceptibility, we find that $1/\chi_{\xi\xi}(\mathbf{Q}, \sigma = 0) = 1/\chi_{\eta\eta}(\mathbf{Q}, 0) = 2A_\xi - \mathcal{J}(\mathbf{Q})$ vanishes at the temperature determined by

$$k_B T_N \simeq \tfrac{1}{3} J(J+1)\mathcal{J}(\mathbf{Q})\big[1 + \tfrac{2}{5}(J - \tfrac{1}{2})(J + \tfrac{3}{2})B_2^0/k_B T_N\big]. \quad (2.1.25)$$

Below T_N, both σ_ξ and σ_η are generally non-zero at the wave-vector $\mathbf{Q}$, and the free energy f, given by (2.1.24) with $\sigma_\zeta = 0$, is minimized when $\sigma_\xi(\mathbf{Q}) = \sigma_\eta(\mathbf{Q}) = \sigma_{\mathbf{Q}}$, and

$$\sigma_{\mathbf{Q}} = \left(\frac{\mathcal{J}(\mathbf{Q}) - 2A_\xi}{4J^2 B_{\xi\xi}}\right)^{1/2} \quad ; \quad \varphi_\xi - \varphi_\eta = \pm\frac{\pi}{2}, \quad (2.1.26a)$$

corresponding to the helical ordering:

$$\begin{aligned} \langle J_{i\xi}\rangle &= J\sigma_{\mathbf{Q}} \cos(\mathbf{Q}\cdot\mathbf{R}_i + \varphi) \\ \langle J_{i\eta}\rangle &= \pm J\sigma_{\mathbf{Q}} \sin(\mathbf{Q}\cdot\mathbf{R}_i + \varphi). \end{aligned} \quad (2.1.26b)$$

The length of the angular-momentum vector is $J\sigma_{\mathbf{Q}}$, independent of the site considered. There are two energetically-degenerate configurations,

a right- or a left-handed screw, depending on the choice of sign. From the condition $1/\chi_{\xi\xi}(\mathbf{Q},0) \propto (T - T_N)$, sufficiently close to T_N, we get the usual MF result that the order parameter $\sigma_{\mathbf{Q}} \propto (T_N - T)^{1/2}$. Although $1/\chi_{\xi\xi}(\mathbf{Q},0)$ becomes negative below T_N, the inverse of the actual susceptibility, $1/\chi_{\xi\xi}(\mathbf{Q}) = 1/\chi_{\xi\xi}(\mathbf{Q},\sigma_{\mathbf{Q}})$, does not. Analogously to the derivation of A_α in (2.1.21a), it may be seen that $1/\chi_{\xi\xi}(\mathbf{Q})$ is a second derivative of the free energy, i.e.

$$\begin{aligned} 1/\chi_{\xi\xi}(\mathbf{Q}) &= \partial^2 f/\partial(J\sigma_{\mathbf{Q}})^2 \\ &\simeq 1/\chi_{\xi\xi}(\mathbf{Q},\sigma=0) + 12J^2 B_{\xi\xi}\sigma_{\mathbf{Q}}^2 = -2/\chi_{\xi\xi}(\mathbf{Q},\sigma=0). \end{aligned}$$

Hence, $1/\chi_{\xi\xi}(\mathbf{Q})$ is non-negative, as it must be to ensure that the system is stable, as is also the case for any other component of the susceptibility.

Because $|\langle\mathbf{J}_i\rangle|$ is constant, the *umklapp* contributions to the free energy in (2.1.24), for which $4Q$ is a multiple of the reciprocal-lattice parameter $4\pi/c$, cancel. The free energy of the helix is therefore independent of the lattice, at least to the fourth power in the magnetization. If the anisotropy terms in $\mathcal{H}_{\rm cf}$ can be neglected, the helix is the most stable configuration satisfying the condition that $|\langle\mathbf{J}_i\rangle| = J\sigma$ is constant. With this constraint, only the two-ion interaction term in the free energy (2.1.22) may vary, and this may be minimized by the method of Lagrange multipliers (Nagamiya 1967). We will begin with the weaker constraint; $\sum_i \langle\mathbf{J}_i\rangle^2 = N(J\sigma)^2$ is constant, which means that we have to minimize the energy expression

$$\begin{aligned} U &= -\frac{1}{2}\sum_{ij}\mathcal{J}(ij)\langle\mathbf{J}_i\rangle\cdot\langle\mathbf{J}_j\rangle + \lambda\sum_i\big(\langle\mathbf{J}_i\rangle^2 - (J\sigma)^2\big) \\ &= N\sum_{\mathbf{q}}\big\{-\tfrac{1}{2}\mathcal{J}(\mathbf{q}) + \lambda\big\}\langle\mathbf{J}(\mathbf{q})\rangle\cdot\langle\mathbf{J}(-\mathbf{q})\rangle - N\lambda(J\sigma)^2, \end{aligned} \qquad (2.1.27a)$$

where the introduction of $\langle\mathbf{J}_i\rangle = \sum_{\mathbf{q}}\langle\mathbf{J}(\mathbf{q})\rangle\exp(i\mathbf{q}\cdot\mathbf{R}_i)$, as in (2.1.10$c$), yields the second form. Minimizing this expression with respect to $\langle\mathbf{J}(-\mathbf{q})\rangle$, we obtain the following equation:

$$\partial U/\partial\langle\mathbf{J}(-\mathbf{q})\rangle = N\big\{-\mathcal{J}(\mathbf{q}) + 2\lambda\big\}\langle\mathbf{J}(\mathbf{q})\rangle = 0,$$

assuming $\mathcal{J}(-\mathbf{q}) = \mathcal{J}(\mathbf{q})$. For a given value of λ, this condition is only satisfied if either $\langle\mathbf{J}(\mathbf{q})\rangle = \mathbf{0}$, or if $\mathbf{q} = \mathbf{q}_\lambda$, where $\mathcal{J}(\mathbf{q}_\lambda) = 2\lambda$, which implies that only $\langle\mathbf{J}(\mathbf{q}_\lambda)\rangle$ may be non-zero. Introducing this condition in U, we find

$$U = -N\lambda(J\sigma)^2 = -\tfrac{1}{2}N\mathcal{J}(\mathbf{q}_\lambda)(J\sigma)^2, \qquad (2.1.27b)$$

which is then minimized with respect to $\mathbf{q}$ when $\mathbf{q}_\lambda = \mathbf{Q}$, at which wave-vector $\mathcal{J}(\mathbf{q})$ has its maximum. Hence the two-ion energy attains its minimum when only the two Fourier components $\langle \mathbf{J}_i(\pm\mathbf{Q})\rangle$ are non-zero. The stronger constraint that $|\langle \mathbf{J}_i\rangle|$ should be constant is then met only by the helix (2.1.26). In the zero-temperature limit, this constraint derives from the fact that the moments attain their saturation value, $|\langle \mathbf{J}_i\rangle| = J$, immediately the exchange field is not identically zero, since $\chi^o_{\alpha\alpha}(\sigma = 0)$ diverges in this limit when $\mathcal{H}_{\rm cf} = 0$. At elevated temperatures, it is clear that the sum of the single-ion terms in the free energy (the A- and B-terms in (2.1.22)) is most effectively minimized if the minimum condition is the same for all the ions. When $\mathcal{H}_{\rm cf} = 0$, there are no restrictions on the plane in which the moments spiral; it may be rotated freely, without change in energy, as long as $|\mathbf{J}_i|$ is constant and all the components vary with the wave-vector $\mathbf{Q}$. This behaviour is analogous to that of the Heisenberg ferromagnet, which may be considered as a helically ordered system with $\mathbf{Q} = \mathbf{0}$. If $\mathbf{Q}$ is not perpendicular to the plane in which the moments lie, the structure is called the *tilted helix* (Elliott 1971; Sherrington 1972) and the extreme case, with $\mathbf{Q}$ in the plane of the moments, is the *cycloidal structure*. When $B_2^0 > 0$, the orientation of the plane is stabilized to be perpendicular to the c-axis, and with $\mathbf{Q}$ along this axis we obtain the true helical structure.

If $B_2^0 > 0$ is the only crystal-field parameter of importance, the regular helix is the stable structure in the whole temperature interval between zero and T_N. If the Landau expansion (2.1.22) is continued to the sixth power in the magnetization, a term appears proportional to B_6^6, distinguishing between the a- and b-directions in the basal-plane. Instead of using this expansion, we shall consider the alternative expression for the free energy, to leading order in B_6^6,

$$\begin{aligned} F &\simeq F_1 - \frac{1}{2}\sum_{ij}\mathcal{J}(ij)\langle \mathbf{J}_i\rangle\cdot\langle \mathbf{J}_j\rangle + \sum_i B_6^6\langle O_6^6(\mathbf{J}_i)\rangle \\ &= F_1 - \frac{1}{2}\sum_{ij}(J\sigma)^2\mathcal{J}(ij)\cos(\phi_i - \phi_j) + \sum_i \kappa_6^6\cos 6\phi_i, \end{aligned} \tag{2.1.28}$$

where $\mathbf{J}_i = J\sigma(\cos\phi_i, \sin\phi_i, 0)$ and F_1 is the part independent of ϕ_i. The expectation values are those obtained in the limit $B_6^6 = 0$, i.e. σ and κ_6^6 are assumed to be independent of the angle ϕ_i. The presence of the six-fold anisotropy term distorts the helix. In order to solve the equilibrium equation

$$\partial F/\partial\phi_i = (J\sigma)^2\sum_j \mathcal{J}(ij)\sin(\phi_i - \phi_j) - 6\kappa_6^6\sin 6\phi_i = 0,$$

we introduce the expansion

$$\phi_i = u_i + \gamma\sin 6u_i + \cdots \qquad ; \quad u_i = \mathbf{Q}\cdot\mathbf{R}_i, \tag{2.1.29a}$$

using the series

$$\begin{aligned}&\exp[i(u+\gamma\sin 6u)]\\&\quad= J_0(\gamma)e^{iu}+J_1(\gamma)\big(e^{i7u}-e^{-i5u}\big)+J_2(\gamma)\big(e^{i13u}+e^{-i11u}\big)+\cdots\\&\quad\simeq e^{iu}+\frac{\gamma}{2}\big(e^{i7u}-e^{-i5u}\big),\end{aligned}\tag{2.1.29b}$$

where $J_n(x)$ are the Bessel functions. To leading order in γ, the equilibrium equation then gives

$$\gamma=\frac{12\kappa_6^6}{(J\sigma)^2\big\{2\mathcal{J}(\mathbf{Q})-\mathcal{J}(5\mathbf{Q})-\mathcal{J}(7\mathbf{Q})\big\}},\tag{2.1.30a}$$

and the free energy is reduced proportionally to γ^2:

$$F/N=F_1/N-\tfrac{1}{2}(J\sigma)^2\mathcal{J}(\mathbf{Q})-\tfrac{1}{8}(J\sigma)^2\big\{2\mathcal{J}(\mathbf{Q})-\mathcal{J}(5\mathbf{Q})-\mathcal{J}(7\mathbf{Q})\big\}\gamma^2.\tag{2.1.30b}$$

The hexagonal anisotropy introduces harmonics, of equal magnitude, in the basal-plane moments at the wave-vectors $6\mathbf{Q}\pm\mathbf{Q}$ and, in higher order, at the wave-vectors $6m\mathbf{Q}\pm\mathbf{Q}$. If κ_6^6, and thus also γ, are negative, the easy directions in the plane are the a-axes. In the special case where the angle $u_i=\pi/12$, i.e. the unperturbed ith moment is half-way between an easy and a hard direction, the largest change $\phi_i-u_i=\gamma$ occurs in the orientation of the moments, and the angle to the nearest easy direction is reduced, since u_i lies between 0 and $\pi/6$, and κ_6^6 is negative. The moments in the helix are therefore distorted so that they bunch around the easy axes.

The above calculation is not valid if Q is 0 or $2\pi/c$, when the hexagonal anisotropy may be minimized without increasing the exchange energy, as it may also if the (average) turn angle ω of the moments from one hexagonal plane to the next is a multiple of 60°, so that $6Q$ is an integer times $4\pi/c$. The products of the fifth and seventh harmonics introduce additional umklapp contributions to the free energy if $12Q$ is a multiple of the *effective* reciprocal-lattice spacing $4\pi/c$, implying that the cases where ω is $p30^\circ$ and $p=1,3,5$ are also special. In higher order, corrections appear whenever $m12Q=p4\pi/c$, where m and p are integers and $0\le p\le 6m$, i.e. at any commensurable value of Q, but the corrections decrease rapidly with m, excluding cases where m and p have common factors. In contrast to the result found above, the commensurable contributions depend on the absolute phase φ in (2.1.26b), and an adjustment of this phase will quite generally allow the system to reduce the anisotropy energy through the umklapp terms. This change in energy may compensate for the increase in the exchange energy when the ordering wave-vector $\mathbf{Q}$ is changed from its value $\mathbf{Q}=\mathbf{Q}_0$, at which

$\mathcal{J}(\mathbf{q})$ has its maximum, to a nearby commensurable value $\mathbf{Q}_c$. Hence the hexagonal anisotropy couples the helical magnetic structure to the lattice, and it may induce continuous or abrupt changes of the ordering wave-vector as a function of temperature, as discussed, for instance, by Bak (1982). In Ho, $12Q_0$ is close to $4\pi/c$, and the hexagonal anisotropy is large at low temperatures. Experimental investigations have shown that a number of commensurable values of $\mathbf{Q}$ are stabilized in this system, as we shall discuss in more detail in the last section of this chapter.

2.1.4 Longitudinally ordered phases

When B_2^0 is negative, as in Er and Tm, $\chi_{\zeta\zeta}(\mathbf{Q})$ is the component of the susceptibility which diverges at the highest temperature, and the high-temperature expansion predicts that $2A_\zeta - \mathcal{J}(\mathbf{Q})$ vanishes at a critical temperature determined by

$$k_B T_N \simeq \tfrac{1}{3} J(J+1)\mathcal{J}(\mathbf{Q})\big[1 - \tfrac{4}{5}(J-\tfrac{1}{2})(J+\tfrac{3}{2})B_2^0/k_B T_N\big]. \quad (2.1.31)$$

Just below this temperature, only the component σ_ζ at the wave-vector $\mathbf{Q}$ is non-zero and, from the free energy expansion (2.1.24), $\partial f/\partial\sigma_\zeta = 0$ determines the relative magnetization as

$$\sigma_\zeta(\mathbf{Q}) = \sigma_{\mathbf{Q}} = \left(\frac{\mathcal{J}(\mathbf{Q}) - 2A_\zeta}{3J^2 B_{\zeta\zeta}}\right)^{1/2}. \quad (2.1.32)$$

The free energy is independent of the phase $\varphi = \varphi_\zeta$, so we set $\varphi = 0$. If we add another Fourier component with $\mathbf{q} \neq \pm\mathbf{Q}$:

$$\langle J_{i\zeta}\rangle = J\sigma_{\mathbf{Q}} \cos(\mathbf{Q}\cdot\mathbf{R}_i) + J\sigma_{\mathbf{q}} \cos(\mathbf{q}\cdot\mathbf{R}_i + \varphi') \quad (2.1.33)$$

then, if $m\mathbf{Q} \pm n\mathbf{q}$ is different from a reciprocal lattice vector, where m and n are integers and $m + n = \pm 4$, the free energy is

$$f = \tfrac{1}{4}J^2\big[\{2A_\zeta - \mathcal{J}(\mathbf{Q})\}\sigma_{\mathbf{Q}}^2 + \{2A_\zeta - \mathcal{J}(\mathbf{q})\}\sigma_{\mathbf{q}}^2\big] + \tfrac{1}{8}J^4 B_{\zeta\zeta}\big[3\sigma_{\mathbf{Q}}^4 + 3\sigma_{\mathbf{q}}^4 + 12\sigma_{\mathbf{Q}}^2\sigma_{\mathbf{q}}^2 + 4\sigma_{\mathbf{Q}}^3\sigma_{\mathbf{q}}\delta_{\mathbf{q},\pm 3\mathbf{Q}}\cos\varphi' + 4\sigma_{\mathbf{Q}}\sigma_{\mathbf{q}}^3\delta_{3\mathbf{q},\pm\mathbf{Q}}\cos 3\varphi'\big]. \quad (2.1.34)$$

This result shows that, if $\mathbf{q} = 3\mathbf{Q}$ or $\mathbf{q} = \frac{1}{3}\mathbf{Q}$, there is an extra fourth-order contribution to the free energy ($\mathbf{q} \to -\mathbf{q}$ represents the same structure with $\varphi' \to -\varphi'$). Of these two special cases, the one where $\mathbf{q} = 3\mathbf{Q}$ is the most interesting, because the extra term is linear in $\sigma_{3\mathbf{Q}}$. This means that the third harmonic appears simultaneously with the basic Fourier component at $\mathbf{Q}$. Minimizing the free energy given by (2.1.34), we find

$$\sigma_{3\mathbf{Q}} = \frac{J^2 B_{\zeta\zeta}}{\mathcal{J}(\mathbf{Q}) - \mathcal{J}(3\mathbf{Q})}\sigma_{\mathbf{Q}}^3 \quad ; \quad \varphi' = \varphi + \pi, \quad (2.1.35a)$$

neglecting a term proportional to $\sigma_{\mathbf{Q}}^2$ in the denominator. The $3\mathbf{Q}$-component is thus proportional to $\sigma_{\mathbf{Q}}^3$, and hence to $(T_N - T)^{3/2}$. Denoting the wave-vector at which $\mathcal{J}(\mathbf{q})$ has its maximum by $\mathbf{Q}_0$, we conclude that the appearance of the third harmonic implies that f has its minimum at a value of $\mathbf{Q}$ slightly different from $\mathbf{Q}_0$. Minimizing the free energy with respect to $\mathbf{Q}$ along the c-axis, by requiring $\partial f/\partial Q = 0$, we obtain to leading order

$$Q = Q_0 - 3\frac{\mathcal{J}'(3\mathbf{Q}_0)}{\mathcal{J}''(\mathbf{Q}_0)}\left(\frac{\sigma_{3\mathbf{Q}}}{\sigma_{\mathbf{Q}}}\right)^2. \tag{2.1.35b}$$

$\mathcal{J}''(\mathbf{Q}_0)$ is negative, so the shift $Q - Q_0$ has the same sign as $\mathcal{J}'(3\mathbf{Q}_0)$ and is proportional to $(T_N - T)^2$. The other special case, $3\mathbf{q} = \mathbf{Q}$, reflects the possibility that, if $\mathcal{J}(\mathbf{Q}_0/3)$ is close to $\mathcal{J}(\mathbf{Q}_0)$, the system may reduce its energy by making a *first order* transition to a state where $\mathbf{Q} \simeq \mathbf{Q}_0/3$ is the fundamental wave-vector, with the third harmonic being close to $\mathbf{Q}_0$. The presence of a term in the free energy cubic in the order parameter, $\sigma_{\mathbf{Q}/3}$ in this case, implies that the transition becomes of first order, so that the order parameter changes discontinuously from zero to a finite value. The $\mathbf{Q}_0/3$-transition appears to be of no importance in real systems, so we shall return to the discussion of the other case. If the free energy is expanded to higher (even) powers in the relative magnetization, it is clear that the $(2n+2)$-power term leads to a contribution proportional to $\sigma_{(2n+1)\mathbf{Q}}\sigma_{\mathbf{Q}}^{2n+1}$ which, in combination with the term quadratic in $\sigma_{(2n+1)\mathbf{Q}}$, implies that the ordering at the fundamental wave-vector $\mathbf{Q}$ induces a $(2n+1)$-harmonic proportional to $\sigma_{\mathbf{Q}}^{2n+1} \propto (T_N - T)^{(2n+1)/2}$. Starting as a pure sinusoidally modulated wave at T_N, the moments approach the *square wave*

$$\langle J_{i\zeta}\rangle = \frac{4J}{\pi}\big(\cos x - \tfrac{1}{3}\cos 3x + \tfrac{1}{5}\cos 5x - \tfrac{1}{7}\cos 7x + \cdots\big)_{x=\mathbf{Q}\cdot\mathbf{R}_i+\varphi}, \tag{2.1.36a}$$

in the limit of zero temperature where $\langle J_{i\zeta}\rangle = \pm J$, neglecting strong anisotropy effects. Although the behaviour of the angular momentum is simple, the dependence of the free energy on the wave-vector is complicated. It is only when the ordering is incommensurable, i.e. mQ is different from any multiple of the length $4\pi/c$ of the reciprocal-lattice vector along the c-axis, that the energy of the square-wave structure at $T = 0$ is

$$f(0) = \langle \mathcal{H}_{\mathrm{cf}}\rangle - \frac{4J^2}{\pi^2}\big\{\mathcal{J}(\mathbf{Q}) + \tfrac{1}{9}\mathcal{J}(3\mathbf{Q}) + \tfrac{1}{25}\mathcal{J}(5\mathbf{Q}) + \cdots\big\}. \tag{2.1.36b}$$

An infinitesimal change of the ordering wave-vector from $\mathbf{Q}$, which minimizes $f(0)$, to $\mathbf{Q}_c$ may make it commensurable with the lattice, so that

$mQ_c = p(4\pi/c)$ and additional umklapp terms contribute to the free energy. Again these contributions depend on the absolute phase φ, and there will always be values of Q_c close to Q leading to a lower free energy than that obtained in the incommensurable case. In the low-temperature limit, the modulation of the c-axis moment is therefore locked to the lattice periodicity. This tendency is already apparent close to T_N. In the expansion of the free energy considered above for $m = 4$, umklapp terms modify the fourth-power coefficient, and analogous effects occur in higher powers of the magnetization. This indicates that the system may stay commensurable even near T_N although, in the close neighbourhood of T_N, the critical fluctuations neglected here may oppose this tendency. The optimal value of Q_c may change as a function of temperature, in which case the system will exhibit a number of first-order, or possibly continuous, transitions from one commensurable structure to another. Of these structures, those for which $Q_c = 3Q_c = 5Q_c = \cdots$, i.e. $Q_c = 0$ or $2\pi/c$, are particularly stable, as they only involve one wave-vector, so that $f(0) = \langle \mathcal{H}_{\rm cf} \rangle - \frac{1}{2}J^2\mathcal{J}(\mathbf{Q}_c)$ (in this connection, we note that $1 + \frac{1}{9} + \frac{1}{25} + \cdots = \pi^2/8$). The anisotropic Ising-model with competing interactions, the so-called *ANNNI* model, is a simplified version of the above, and it shows a rich variety of different incommensurable, commensurable, and chaotic ordered structures as a function of temperature and the coupling parameters (Bak 1982).

2.1.5 Competing interactions and structures

The complex behaviour of the longitudinally ordered phase is a consequence of the competition between the single-ion part of the free energy, which favours a structure in which the magnitude of the moments varies as little as possible, particularly at low temperature, and the two-ion contributions, which prefer a single-$\mathbf{Q}$ ordering. When B_2^0 is positive, helical ordering satisfies both tendencies without conflict. This points to another alternative which the longitudinal system may choose. Although $\chi_{\zeta\zeta}(\mathbf{Q})$ decreases below T_N, the two perpendicular components continue to increase, and they may therefore diverge at a lower temperature T_N'. Assuming the expansion (2.1.24) of the free energy still to be valid at T_N', and neglecting the third and higher harmonics of $\langle J_{i\zeta} \rangle$, we may write it:

$$f = f(\sigma_{\mathbf{Q}}) + \tfrac{1}{4}J^2 \sum_{\alpha=\xi,\eta} \big[2A_\xi - \mathcal{J}(\mathbf{Q}) + B_{\xi\zeta}(J\sigma_{\mathbf{Q}})^2\{2 + \cos 2(\varphi_\alpha - \varphi)\}\big]\sigma_\alpha^2 + \tfrac{1}{8}J^4 B_{\xi\xi}\big[3\sigma_\xi^4 + 3\sigma_\eta^4 + 2\{2 + \cos 2(\varphi_\xi - \varphi_\eta)\}\sigma_\xi^2\sigma_\eta^2\big]. \quad (2.1.37)$$

The effective coefficient of σ_α^2 ($\alpha = \xi$ or η) is smallest when $\varphi_\alpha = \varphi \pm \frac{\pi}{2}$, meaning that the basal-plane moments appearing just below T_N', where

this coefficient vanishes, are locked to be out of phase by 90° with the c-axis component. This phase difference arises because the transverse MF susceptibility $\chi^o_{\xi\xi}$ for the single sites increases as the c-axis exchange field falls. Using the estimate (2.1.21b) for the B-tensor, and the high-temperature value for A_ξ, we find the transition temperature to be

$$k_B T'_N \simeq \tfrac{1}{3} J(J+1)\mathcal{J}(\mathbf{Q})\Big[1 + \tfrac{2}{5}(J-\tfrac{1}{2})(J+\tfrac{3}{2})B^0_2/k_B T'_N - \tfrac{3}{20}\{1+\tfrac{1}{2}(J+1)^{-2}\}\sigma^2_{\mathbf{Q}}\Big]. \tag{2.1.38}$$

A slightly better estimate may be obtained by calculating the MF value of the transverse susceptibility directly, in the presence of a non-zero exchange field, which just causes the replacement of $\sigma_{\mathbf{Q}}$ in (2.1.38) by $3\sigma_{\mathbf{Q}}\mathcal{J}(\mathbf{Q})/[J(J+1)k_B T'_N]$ (Miwa and Yosida 1961). However, both results are based on the high-temperature expansion, which ceases to be valid at low temperatures. In the zero-temperature limit, $\chi^o_{\xi\xi}$ of the ith site remains finite, being of the order $J/h^{\rm eff}_{i\zeta}$. This saturation implies that the transition does not necessarily occur. If the c-axis is favoured too strongly by the anisotropy terms, the basal-plane components remain disordered at low temperatures, as is observed in Tm. When the basal-plane moments order, as in Er, eqn (2.1.38) may give a reasonable estimate of the transition temperature. As mentioned previously, the modulation of the basal-plane moments, just below T'_N, is locked at 90° out of phase with that of the c-axis component. Since this applies to both components, only a linearly-polarized moment can develop at the transition temperature, with a relative magnitude $\sigma_\perp = (\sigma^2_\xi + \sigma^2_\eta)^{1/2}$, in a specified but arbitrary direction in the plane. If the sixth-power terms are included in the free energy, B^6_6 favours either the a- or the b-directions, but there are still six equivalent but different directions of the moments in the basal plane with equal energies. To be specific, we may assume that B^6_6 is negative and that the ordered moments in the basal plane establish themselves along the ξ-axis. In this case, the moments all lie in the ξ–ζ plane in an elliptic cycloidal structure. Displaced to a common origin, the hodograph of the moments is an ellipse, with its principal axes along the ξ- and ζ-axes, as is illustrated, in connection with our discussion of Er, in Fig. 2.6 on page 120. The c-axis moments will still show a strong tendency towards squaring up with decreasing temperature, as long as they are large compared with the basal-plane moments. Because of the phase-locking between the components, the higher odd-harmonics in the modulation of the c-axis moments will also be reflected in the basal-plane.

At high temperatures, B^0_2 is the dominant anisotropy parameter, and its sign determines whether the system orders in a helically or longitudinally polarized structure, when $\mathbf{Q}_0$ is along the c-axis. If B^0_2 is still

the most important axial-anisotropy parameter in the low-temperature limit, the helix is still a stable structure at $T = 0$ whereas, in the longitudinally polarized case, the tendency to minimize the variation of the lengths of the moments may result in two different paths. Either the system stays in the longitudinally polarized phase, ending up as a (commensurable) square-wave structure at $T = 0$, or it goes through a transition to an elliptic cycloidal structure. The path which is chosen depends on the magnitude of B_2^0; if the effective axial anisotropy $-B_2^0\langle O_2^0\rangle$ is sufficiently large, the ordering of the basal-plane moments is quenched. It has already been mentioned in Section 1.5 that this anisotropy depends on the magnetization, being proportional approximately to σ^3. We shall discuss this renormalization in more detail in the next section, but it is worth mentioning here that this behaviour of the effective anisotropy-parameter means that there is an intermediate range of B_2^0 for which the system makes a transition to the elliptic cycloidal structure, but leaves it again at a lower temperature, by returning to the longitudinally polarized phase when $-B_2^0\langle O_2^0\rangle$ becomes large enough. When B_4^0 and B_6^0 are included, a more realistic situation may occur, in which the low-temperature anisotropy favours an orientation of the moments making an angle θ with the c-axis, which is neither 0 or $\pi/2$ but some, temperature-dependent, intermediate value. In the case of the helix, this means that there will be a critical temperature T_N' (below T_N) where the effective axial anisotropy parameter vanishes, and below which the c-axis moments are ordered. If the ordering wave-vector for the c-axis component is the same as the helical wave-vector, the structure adopted is the tilted helix. However the two-ion coupling between the c-axis moments, $\mathcal{J}_\parallel(\mathbf{q})$ with $\mathbf{q} \parallel c$-axis, is not restricted by any symmetry argument to be equal to the coupling between the basal-plane moments, $\mathcal{J}_\perp(\mathbf{q}) = \mathcal{J}(\mathbf{q})$ with its maximum at $\mathbf{q} = \mathbf{Q}_0$. If the maximum of $\mathcal{J}_\parallel(\mathbf{q})$ lies at a $\mathbf{q} \neq \mathbf{Q}_0$, the c-component will order at this wave-vector and not at $\mathbf{Q}_0$, as the extra energy gained by the c-component by locking to the basal-plane moments is very small, being proportional to $\{B_6^6\langle O_6^6\rangle/(J\sigma)^2\mathcal{J}(\mathbf{Q})\}^2$. When B_2^0 is negative, a non-zero value of θ favours the elliptic cycloidal structure, compared to the longitudinally polarized phase. If the system is already in the cycloidal phase, it may undergo a new second-order transition, in which the plane of the ellipse starts to tilt away from the ξ–ζ plane, in close correspondence with the behaviour of the helix. Referring back to eqn (2.1.37), we observe that this transition occurs when the coefficient of σ_η^2, with $\varphi_\eta = \varphi\,(+\pi) = \varphi_\xi \pm \pi/2$, becomes zero. The phase-locking energy, comprising the terms in (2.1.37) involving φ_η, is more important in this case than in the helix, but it is nevertheless possible that the third component may order at a wave-vector different from that of the other

two. If the η-component is locked at the same wave-vector as the two other components, and if the ellipse is tilted just such an amount that $\sigma_\eta = \sigma_\xi$, the structure is a helix superimposed on a modulated c-axis moment. If a transition to the tilted cycloidal structure has occurred, and the hexagonal anisotropy is small, it might be favourable for the system at a lower temperature to pass directly, via a first-order transition, to this helical structure in which the c-axis component is no longer phase-locked to the basal-plane moments.

Instead of basing our analysis on the Hamiltonian (2.1.1), we may use symmetry arguments for deriving the most general behaviour of the magnetic ordering in hcp crystals. We have already indicated that $\mathcal{J}_\parallel(\mathbf{q})$ may differ from $\mathcal{J}_\perp(\mathbf{q})$ and mentioned some of the consequences. The assumption that the c-axis is effectively a six-fold axis of the lattice leads to the strong restriction that the expansion of the free energy, (2.1.22) or (2.1.24), only involves even powers of each of the Cartesian components, when $\mathbf{q}$ is along this axis. This has the consequence, for example, that all the main transitions, at T_N or T'_N, are predicted to be of second order, excluding those involving changes of the same component, i.e. transitions between different commensurable structures. However, there are two-ion terms which reflect the fact that the c-axis is only a three-fold axis. The term of lowest rank has the form

$$\mathcal{H}_3(i \in s\text{'th plane}) = (-1)^s K_3 \Big[(J_{i\zeta} - \tfrac{1}{2}\langle J_{i\zeta}\rangle)\big\langle O_3^{-3}(\mathbf{J}_{s+1}) - O_3^{-3}(\mathbf{J}_{s-1})\big\rangle + (O_3^{-3}(\mathbf{J}_i) - \tfrac{1}{2}\langle O_3^{-3}(\mathbf{J}_i)\rangle)\big\langle J_{s+1,\zeta} - J_{s-1,\zeta}\big\rangle \Big], \quad (2.1.39)$$

in the MF approximation, where only interactions between neighbouring planes are included. $O_3^{-3} = (J_+^3 - J_-^3)/2i$, and $\mathbf{J}_{s\pm1}$ denotes a moment in the $(s\pm1)$th plane. The contribution of this coupling to the expansion (2.1.22) of the free energy to the fourth power is found by adding $\sum_i \langle \mathcal{H}_3 \rangle$ to F, using the approximation $\langle O_3^{-3}(\mathbf{J}_i)\rangle \propto \langle J_{i\eta}\rangle(3\langle J_{i\xi}\rangle^2 - \langle J_{i\eta}\rangle^2) = \langle J_\perp\rangle^3 \sin 3\phi_i$. One remarkable effect is that this coupling introduces a term linear in $\langle J_{i\zeta}\rangle$ in the helix. If the basal-plane moments are ordered with the wave-vector $\mathbf{Q}$, they induce a c-axis moment modulated with a wave-vector along the c-axis of length $2\pi/c - 3Q$, provided that $6\mathbf{Q}$ is not a reciprocal lattice vector. In the elliptic cycloidal structure, this coupling induces an ordering of the η-component at the two wave-vectors of length $2\pi/c - Q$ and $2\pi/c - 3Q$, when the ellipse is assumed to lie in the ξ–ζ plane and only the fundamental at Q is considered. Although this additional coupling may not change the nature of the transitions at T_N or T'_N, it has qualitative consequences for the magnetic structures, and it may introduce new effects associated with commensurability. For instance, the three-fold symmetrical interaction will favour the commensurable structure with $Q = \pi/2c$ (an average turn angle of 45°). In the

case of a helix with this particular period, the coupling induces a modulation of the c-axis moments with the same wave-vector, $2\pi/c - 3Q = Q$, causing a tilting of the plane of the helix.

2.1.6 Multiply periodic structures

We have so far only considered order parameters which are specified by two $\mathbf{Q}$-vectors ($\pm\mathbf{Q}$), or one $\mathbf{Q}$ plus a phase. This is a consequence of the assumption that $\mathbf{Q}$ is along the c-axis. If $\mathbf{Q}$ is in the basal-plane, as in the light rare earths Pr and Nd, there are six equivalent ordering wave-vectors, $\pm\mathbf{Q}_1$, $\pm\mathbf{Q}_2$, and $\pm\mathbf{Q}_3$, where the three vectors make an angle of 120° with each other. This leads to the possibility that the ordered structure is a *multiple-*$\mathbf{Q}$ *structure*, where

$$\langle \mathbf{J}_i \rangle = \mathbf{J}_1 \cos(\mathbf{Q}_1 \cdot \mathbf{R}_i + \varphi_1) + \mathbf{J}_2 \cos(\mathbf{Q}_2 \cdot \mathbf{R}_i + \varphi_2) + \mathbf{J}_3 \cos(\mathbf{Q}_3 \cdot \mathbf{R}_i + \varphi_3) \tag{2.1.40}$$

referred to as *single-, double-,* or *triple-*$\mathbf{Q}$ ordering, depending on the number of vectors $\mathbf{J}_p$ which are non-zero. The transition at T_N will generally involve only a single real vector $\mathbf{J}_p$ for each $\mathbf{Q}_p$, as implicitly assumed in (2.1.40). We will not therefore consider multiple-$\mathbf{Q}$ cycloidal/helical structures, but restrict the discussion to configurations which correspond to the type observed in Pr or Nd. We furthermore neglect the complications due to the occurrence of different sublattices in the dhcp crystals, by assuming the lattice to be primitive hexagonal. This simplification does not affect the description of the main features of the magnetic structures. On the hexagonal sites of Pr and Nd, the ordered moments below T_N lie in the basal plane. This confinement is not primarily determined by the sign of B_2^0, but is decisively influenced by the anisotropic two-ion coupling

$$\mathcal{H}_{\text{an}} = \frac{1}{2} \sum_{ij} \mathcal{K}(ij) \left[(J_{i\xi} J_{j\xi} - J_{i\eta} J_{j\eta}) \cos 2\phi_{ij} + (J_{i\xi} J_{j\eta} + J_{i\eta} J_{j\xi}) \sin 2\phi_{ij} \right], \tag{2.1.41}$$

where ϕ_{ij} is the angle between the ξ-axis and the projection of $\mathbf{R}_i - \mathbf{R}_j$ on the basal plane. This anisotropic coupling, which includes a minor contribution from the classical dipole–dipole interaction, is known from the excitation spectrum to be of the same order of magnitude as the isotropic coupling in Pr, as we shall discuss in Chapter 7, and must be of comparable importance in Nd. We define the coupling parameter $\mathcal{K}(\mathbf{q}) = \mathcal{K}_0(q) + \mathcal{K}_6(q) \cos 6\psi_q$, where ψ_q is the angle between $\mathbf{q}$ (in the basal plane) and the ξ-axis, and $\mathcal{K}_0(q) \pm \mathcal{K}_6(q)$ is the Fourier transform of $\pm\mathcal{K}(ij) \cos 2\phi_{ij}$ when $\mathbf{q}$ is respectively parallel or perpendicular to the ξ-axis. Introducing $\mathbf{J}_p = J\boldsymbol{\sigma}_p$, and assuming the moments to be perpendicular to the c-axis, we find the mean-field free energy of second

order in σ_p to be

$$f_2(\sigma_p) = \tfrac{1}{4}J^2 \sum_p \big[\{2A_\xi - \mathcal{J}(\mathbf{Q}_p)\}\sigma_p^2 + \mathcal{K}(\mathbf{Q}_p)\{2(\boldsymbol{\sigma}_p \cdot \hat{\mathbf{Q}}_p)^2 - \sigma_p^2\}\big], \tag{2.1.42}$$

where $\hat{\mathbf{Q}}_p = \mathbf{Q}_p/Q_p$. In Pr and Nd, the maximum of $\mathcal{J}(\mathbf{q}) \pm \mathcal{K}(\mathbf{q})$ is found at $\mathbf{q} = \mathbf{Q}$ along the η-axis, or the other equivalent b-axes, with Q being about one fourth of the distance to the Brillouin-zone boundary, and $\mathcal{K}(\mathbf{Q})$ is negative. The transition between the paramagnetic phase and a phase described by (2.1.40), with $\mathbf{J}_p$ lying in the hexagonal plane, then occurs when the coefficient $2A_\xi - \mathcal{J}(\mathbf{Q}) + \mathcal{K}(\mathbf{Q})$ vanishes, at which temperature the corresponding factor for the c-component of the moments, $2A_\zeta - \mathcal{J}(\mathbf{Q})$, is still positive in Pr and Nd. Besides confining the moments to the hexagonal planes, $\mathcal{K}(\mathbf{Q})$ also removes the degeneracy between the two states in which $\mathbf{J}_p$ is parallel or perpendicular to $\mathbf{Q}_p$. With a negative $\mathcal{K}(\mathbf{Q})$, the anisotropic coupling favours a longitudinal ordering of the moments at T_N, with $\mathbf{J}_p$ parallel to $\mathbf{Q}_p$. Just below T_N, the magnitude of the ordered moments is determined by $f_2(\sigma_p)$, together with the fourth-order contributions. When the moments lie in the basal plane ($B = B_{\xi\xi} = B_{\eta\eta} = B_{\xi\eta}$), we obtain, from eqn (2.1.22),

$$\begin{aligned} f_4(\sigma_p) &= B\frac{1}{N}\sum_i \big(\langle \mathbf{J}_i \rangle \cdot \langle \mathbf{J}_i \rangle\big)^2 \\ &= BJ^4\Big[\tfrac{3}{8}\sum_p \sigma_p^4 + \tfrac{1}{4}\sum_{p\neq p'} \big\{\sigma_p^2\sigma_{p'}^2 + 2(\boldsymbol{\sigma}_p \cdot \boldsymbol{\sigma}_{p'})^2\big\}\Big]. \end{aligned} \tag{2.1.43}$$

Introducing the effective order parameter σ, defined by $\sigma^2 = \sum_p \sigma_p^2$, we obtain further:

$$f \simeq f_2(\sigma_p) + f_4(\sigma_p) = \tfrac{1}{4}J^2\big\{2A_\xi - \mathcal{J}(\mathbf{Q}) + \mathcal{K}(\mathbf{Q})\big\}\,\sigma^2 + \tfrac{3}{8}J^4 B\,\sigma^4, \tag{2.1.44}$$

assuming $\mathbf{J}_p$ parallel to $\mathbf{Q}_p$ along the three b-axes making an angle of 120° with each other ($\hat{\mathbf{Q}}_p \cdot \hat{\mathbf{Q}}_{p'} = -1/2$ when $p \neq p'$). Hence the free energy, in this approximation, is independent of whether the ordering is single-, double- or triple-$\mathbf{Q}$. Instead of utilizing (2.1.22), we may appeal to symmetry arguments, by which the fourth-order term may readily be seen to have the general form

$$f_4(\sigma_p) = u\sum_p \sigma_p^4 + \tfrac{1}{2}v\sum_{p\neq p'} \sigma_p^2\sigma_{p'}^2, \tag{2.1.45a}$$

as long as the angles between the different $\boldsymbol{\sigma}_p$ vectors remain at 120° (Bak and Lebech 1978). Introducing the parameter $w \equiv v - 2u$, we may write this:

$$f_4(\sigma_p) = u\big(\sum_p \sigma_p^2\big)^2 + \tfrac{1}{2}w\sum_{p\neq p'} \sigma_p^2\sigma_{p'}^2 = (u + \gamma w)\sigma^4, \tag{2.1.45b}$$

where $\gamma = 0$, $1/4$, or $1/3$ respectively, in a single-, double-, or triple-**Q** structure. If only an isotropic two-ion coupling and the crystal-field terms are included, $2u = v$ or $w = 0$, and the different multiple-**Q** structures are degenerate to the fourth power of the order parameter. This situation is not changed by the anisotropic dipole coupling $\mathcal{K}(\mathbf{q})$ introduced above (as long as $\boldsymbol{\sigma}_p$ is parallel to $\mathbf{Q}_p$). However, two-ion quadrupole couplings may remove the degeneracy. For example, the coupling $\mathcal{K}_2(ij)J_{i+}^2 J_{j-}^2$ makes a contribution proportional to

$$w \sim 3\mathcal{K}_2(\mathbf{0}) + \mathcal{K}_2(2\mathbf{Q}) - 2\mathcal{K}_2(\mathbf{Q}) - 2\mathcal{K}_2(\mathbf{Q}_1 - \mathbf{Q}_2). \tag{2.1.46}$$

Depending on the detailed **q**-dependence of this coupling, it may lead to a positive or a negative contribution to w. If w is positive, the single-**Q** structure is stable, and conversely a negative w leads to a triple-**Q** structure just below T_N. The Landau expansion for this case has been discussed by Forgan (1982), Walker and McEwen (1983) and McEwen and Walker (1986), who all take the possible contributions to w as being of magnetoelastic origin. In Pr, the dominating magnetoelastic interaction is known to be due to the γ-strain coupling, and a rough estimate (including both the uniform and modulated γ-strain) indicates that v is unaffected, whereas the reduction of u proportional to $B_{\gamma 2}^2/c_\gamma$, with the parameters of (1.5.27), is about 10%, corresponding to a *positive* contribution to w of about $0.2u$, or to an energy difference between the single- and double-**Q** structures of $\sim 0.05u\sigma^4$. If the other quadrupolar contributions are unimportant, as is indicated by the behaviour of the excitations in Pr (Houmann *et al.* 1979), we should expect the single-**Q** structure to be favoured in Pr and Nd, at least close to T_N.

If w is relatively small, the single- or triple-**Q** structures may only be stable in a narrow temperature range below T_N, because the sixth-order contributions may assume a decisive influence. A number of new effects appear in this order, but the most important stems from the possibility that the moments and the wave-vectors may rotate away from the b-directions, as first considered by Forgan (1982). The $(\boldsymbol{\sigma}_p \cdot \boldsymbol{\sigma}_{p'})^2$-term in (2.1.43) may drive such a rotation, because it favours an orthogonal configuration of the different $\boldsymbol{\sigma}_p$ vectors, since B is positive. This term does not appear in the single-**Q** structure, whereas in the triple-**Q** case, $f_4(\sigma_p)$ is reduced quadratically with θ_p, where θ_p is the angle between $\mathbf{J}_p$ and the nearest b-direction. However, the much larger quadratic increase of $f_2(\sigma_p)$, due to $\mathcal{K}(\mathbf{Q})$, will eliminate any tendency for θ_p to become non-zero. In contrast, $f_4(\sigma_p)$ depends linearly on θ_p in the double-**Q** structure, and the free energy can always be reduced by allowing the two components $\boldsymbol{\sigma}_1$ and $\boldsymbol{\sigma}_2$ (with $\boldsymbol{\sigma}_3 = \mathbf{0}$) to rotate towards each other. Defining $\mathcal{J}_6(Q)$ equivalently to $\mathcal{K}_6(Q)$, i.e. $\mathcal{J}(\mathbf{Q}) = \mathcal{J}_0(Q) + \mathcal{J}_6(Q)\cos 6\psi_Q$, and using the constraint that the change of ψ_Q for the pth component must

have the same sign as θ_p, we may write the angular-dependent part of the free energy, to the fourth power of the magnetization, as

$$f(\theta,\psi) = \tfrac{1}{4}J^2\big[-\mathcal{J}_6(Q)+\mathcal{K}_6(Q)\cos 2(\theta-\psi)\big] \times\{\sigma_1^2\cos(\pi+6\psi)+\sigma_2^2\cos(5\pi-6\psi)\} +\tfrac{1}{4}J^2\mathcal{K}_0(Q)(\sigma_1^2+\sigma_2^2)\cos 2(\theta-\psi)+BJ^4\sigma_1^2\sigma_2^2\cos^2(2\pi/3-2\theta). \tag{2.1.47a}$$

For definiteness, we have chosen the case where the angle between the ξ-axis and $\boldsymbol{\sigma}_1$ or $\boldsymbol{\sigma}_2$ is respectively $\pi/6+\theta$ and $5\pi/6-\theta$ (by symmetry $\theta=\theta_1=-\theta_2$). Analogously to θ, ψ is the angle between $\mathbf{Q}_p$ and the nearest b-axis. Introducing $\sigma^2=2\sigma_1^2=2\sigma_2^2$, and expanding $f(\theta,\psi)$ to second order in the small angles, we obtain

$$f(\theta,\psi) = f_0-\tfrac{9}{2}(J\sigma)^2\{\mathcal{J}_6(Q)-\mathcal{K}_6(Q)\}\,\psi^2-\tfrac{1}{2}(J\sigma)^2\mathcal{K}(\mathbf{Q})(\theta-\psi)^2 -\tfrac{1}{4}(J\sigma)^4B(\sqrt{3}\theta-2\theta^2). \tag{2.1.47b}$$

We note that, with the chosen sign conventions, $\mathcal{K}(\mathbf{Q})=\mathcal{K}_0(Q)-\mathcal{K}_6(Q)$ and $\mathcal{J}_6(Q)-\mathcal{K}_6(Q)$ are both negative. The additional contribution to the free energy of the double-$\mathbf{Q}$ structure is minimized when

$$\theta=\frac{\sqrt{3}B(J\sigma)^2}{4|\mathcal{K}(\mathbf{Q})|}+\psi \qquad ; \quad \psi=\frac{\sqrt{3}B(J\sigma)^2}{36|\mathcal{J}_6(Q)-\mathcal{K}_6(Q)|}, \tag{2.1.48a}$$

neglecting the small term proportional to $B\theta^2$, in which case

$$\Delta f=-\tfrac{3}{32}B^2(J\sigma)^6\bigg(-\frac{1}{\mathcal{K}(\mathbf{Q})}-\frac{1}{9}\frac{1}{\mathcal{J}_6(Q)-\mathcal{K}_6(Q)}\bigg). \tag{2.1.48b}$$

Introducing $A=A_\xi(T=T_N)$, i.e. $\mathcal{J}(\mathbf{Q})-\mathcal{K}(\mathbf{Q})=2A$, then for Pr we have: $\mathcal{K}(\mathbf{Q})\simeq -0.24A$, $\mathcal{J}_6(Q)-\mathcal{K}_6(Q)\simeq -0.05A$, and $BJ^2\simeq 0.35A$. These values may also provide a reasonable estimate in the case of Nd. Inserting them in (2.1.48), we find that $\theta\simeq 3\psi\simeq 1.0\sigma^2$, and $\Delta f\simeq -0.2BJ^4\sigma^6\simeq -0.5u\sigma^6$. So, even though Δf is of sixth order in σ, it outweighs the small fourth-order energy difference of $w\sigma^4/4$ between the single- and the double-$\mathbf{Q}$ structure when $\sigma^2\approx 0.1$, if $w\simeq 0.2u$ as estimated above. The temperature T_N' at which this occurs is $\sim 0.97\,T_N$, i.e. $\sim 0.9\,\mathrm{K}$ below T_N in Nd. Hence, if w is positive and has the estimated small magnitude, the system will first undergo a second-order transition from the paramagnetic phase to a single-$\mathbf{Q}$ structure, which will only be stable as long as σ^2 is small. At T_N', slightly below T_N, the system will make a first-order transition to a double-$\mathbf{Q}$ structure, in which the moments $\mathbf{J}_1$ and $\mathbf{J}_2$ are rotated slightly towards each other and away from the symmetry axes, as also are the ordering wave-vectors $\mathbf{Q}_1$ and $\mathbf{Q}_2$. These rotations are proportional to σ^2.

The explicitly sixth-order contribution to the free energy, proportional to $(1/N)\sum_i(\langle\mathbf{J}_i\rangle\cdot\langle\mathbf{J}_i\rangle)^3$, is somewhat smaller than the estimated value of Δf, and it leads to energy differences between the different multiple-$\mathbf{Q}$ structures which are a further order of magnitude smaller. The hexagonal-anisotropy term, which also appears in this order, is minute compared to the anisotropy introduced by $\mathcal{K}(\mathbf{Q})$ in Pr and Nd, and its influence on the turn angles ψ and θ should be negligible. The only other new effect in this order is the appearance of higher harmonics. The mechanism is identical to that discussed in Section 2.1.4 for the longitudinally-polarized phase, but in addition to the occurrence of third harmonics at the wave-vectors $3\mathbf{Q}_p$, equivalently to (2.1.35a), they also appear at all possible combinations of $2\mathbf{Q}_p \pm \mathbf{Q}_{p'}$ $(p \neq p')$ in the multiple-$\mathbf{Q}$ structures. In the triple-$\mathbf{Q}$ structure, one might expect third harmonics also at $\mathbf{Q}_1 \pm \mathbf{Q}_2 \pm \mathbf{Q}_3$, but the new wave-vectors derived from this condition are either $\mathbf{0}$, which changes the symmetry class of the system, or twice one of the fundamental wave-vectors, which are energetically unfavourable because they do not contribute to the 'squaring up'. These extra possibilities in the triple-$\mathbf{Q}$ case are not therefore realized. The appearance of the higher 'odd' harmonics is not important for the energy differences between the different multiple-$\mathbf{Q}$ structures, but they may provide an experimental method for differentiating between the various possibilities (Forgan *et al.* 1989). In a neutron-diffraction experiment, the scattering intensity at the fundamental wave-vectors in a multi-domain single-$\mathbf{Q}$ structure, with an equal distribution of the domains, is the same as that produced by a triple-$\mathbf{Q}$ structure. These structures may then be distinguished either by removing some of the domains by applying an external field, or by using scattering peaks at, for instance, $2\mathbf{Q}_1 \pm \mathbf{Q}_2$ to exclude the possibility of a single-$\mathbf{Q}$ structure.

The discussion of this section has been based exclusively on the MF approximation, which neglects the important dynamical feature that a system close to a second-order phase-transition will show strong correlated fluctuations in the components which order at the transition. A discussion of the effects of the *critical fluctuations* is beyond the scope of this book, and we refer instead to the recent introduction to the field by Collins (1989), in which references may be found to the copious literature on the subject. Although the MF approximation does not take into account the contributions to the free energy from the critical fluctuations, it gives a reasonable estimate of the transition temperatures in the rare earth metals, which can all be characterized as three-dimensional systems with long-range interactions. The fluctuations contribute to the free energy on both sides of the transition, and they only suppress the transition temperature by a few per cent in such systems. The Landau expansion considered above does not predict the right *critical*

exponents, but it is nevertheless decisive for which *universality classes* the phase transitions belong to. The transitions which are predicted to be continuous by the MF theory, i.e. all those considered above which are not accompanied by a change of $\mathbf{Q}$ to a commensurable value, may be driven into (weak) first-order behaviour by the fluctuations. An important parameter for determining the nature of the phase transition is the product (n) of the number of components of the order parameter, and of the star of the wave-vector (Mukamel and Krinsky 1976; Bak and Mukamel 1976), the latter being two, corresponding to $\pm\mathbf{Q}$, for the periodically-ordered heavy rare earths. If $n \leq 3$, the transition is expected to remain continuous, which is in accord with the observation by Habenschuss *et al.* (1974) of a second-order transition in Er, since $n = 2$ for the transition between the paramagnetic and the longitudinally ordered phase. The transition from the paramagnet to the helix is less clear-cut, since it belongs to the class $n = 4$, and a theoretical analysis by Barak and Walker (1982) suggested that it might be discontinuous. The bulk of the experimental evidence points towards a continuous transition (Brits and du Plessis 1988) but some measurements, especially by Zochowski *et al.* (1986) on pure Dy, indicate a very weak discontinuity. In the case of the multiple-$\mathbf{Q}$ structures, the fluctuations may drive the transition to the single-$\mathbf{Q}$ structure to be discontinuous, whereas that to the triple-$\mathbf{Q}$ structure, if it is stable, should stay continuous (Bak and Lebech 1978). In Nd, for example, a single-$\mathbf{Q}$ state is formed at T_N and the transition is found to be weakly discontinuous (Zochowski and McEwen 1986). In accordance with the MF analysis above, a first-order transition leads to a double-$\mathbf{Q}$ structure less than a degree below T_N (McEwen *et al.* 1985).

2.2 The magnetic anisotropy

In this section, we shall discuss the thermal expectation-values of the Stevens operators of the single ions when their moments are non-zero, so that $|\langle \mathbf{J}_i \rangle| = \sigma J$. We shall then consider the contribution which the single-ion terms in the Hamiltonian make to the free energy, and thereby derive the relationship between the microscopic parameters and the macroscopic magnetic-anisotropy and magnetoelastic coefficients.

2.2.1 Temperature dependence of the Stevens operators

In a ferromagnet, the *Zener power-law* (1.5.15) for the expectation values of the Stevens operators is valid only at the lowest temperatures. Callen and Callen (1960, 1965) have derived $\langle O_l^m \rangle$ in exchange-dominated systems and obtained results which are useful over a much wider temperature range than the Zener expression. They begin with the density matrix for a single site in the MF approximation, including only the

exchange and Zeeman energies,

$$\rho_{\mathrm{MF}}(x) = \frac{1}{Z}\exp(xJ_z/J) \qquad ; \quad x = \beta\{\mathcal{J}(\mathbf{0})J^2\sigma + g\mu_B JH\}, \quad (2.2.1)$$

where $\sigma = M/M_0$ is the relative magnetization, the direction of which is assumed to be parallel to the field. In this case the nth moment of J_z is determined as

$$\sigma_n = \langle (J_z/J)^n \rangle = \frac{1}{Z}\sum_{p=-J}^{J} \big(\frac{p}{J}\big)^n \exp(xp/J). \quad (2.2.2)$$

This equation offers the possibility of relating the higher moments σ_n to the first moment, which is the relative magnetization $\sigma_1 = \sigma$, without referring explicitly to the MF value of x in eqn (2.2.1). According to the analysis of Callen and Shtrikman (1965), the functional dependence of σ_n on σ has a wider regime of validity than the MF approximation, because it only utilizes the exponential form of the density matrix, which is still valid when correlation effects are included in the random-phase approximation, where the excitations are collective spin-waves, as we shall discuss in Section 3.5. Furthermore, they found that the functions $\sigma_n = \sigma_n(\sigma)$; $n \geq 2$, derived from (2.2.2), only depend very weakly on the actual value of J, and for increasing values these functions rapidly converge towards the results obtained in the limit of infinite J (Callen and Callen 1965). In this limit, the sums in (2.2.2) are replaced by integrals, and the reduced diagonal matrix-elements of the Stevens operators are

$$(1/J^{(l)}) < J_z = p \,|\, O_l^m \,|\, J_z = p > \big|_{J\to\infty} = \delta_{m0} c_l P_l(u = p/J), \quad (2.2.3)$$

where the $J^{(l)}$ are defined by eqn (1.5.25), $P_l(u)$ are the Legendre polynomials, and c_l are constants. Multiplying the terms in the sum in (2.2.2) by $\Delta p = J\Delta u = 1$, and then taking the limit $J \to \infty$, we obtain

$$\frac{1}{c_l J^{(l)}}\langle O_l^0 \rangle = \int_{-1}^{1} P_l(u) e^{xu} du \Big/ \int_{-1}^{1} e^{xu} du = I_{l+\frac{1}{2}}(x)/I_{\frac{1}{2}}(x) = \hat{I}_{l+\frac{1}{2}}(x). \quad (2.2.4)$$

$\hat{I}_{l+\frac{1}{2}}(x)$ is the usual shorthand notation for the ratio of $I_{l+\frac{1}{2}}(x)$ to $I_{\frac{1}{2}}(x)$, and the functions $I_{l+\frac{1}{2}}(x) = (-i)^{l+\frac{1}{2}} J_{l+\frac{1}{2}}(ix)$ are the modified spherical (or hyperbolic) Bessel functions. The relative magnetization

$$\sigma = \hat{I}_{\frac{3}{2}}(x) = \coth x - \frac{1}{x}$$

is the familiar Langevin function $\mathcal{L}(x)$ and, eliminating x in (2.2.4) by writing $x = \mathcal{L}^{-1}(\sigma)$, we finally arrive at

$$\langle O_l^m(\sigma) \rangle = \delta_{m0} c_l J^{(l)} \hat{I}_{l+\frac{1}{2}}[\sigma] \qquad \text{with} \quad \hat{I}_{l+\frac{1}{2}}[\sigma] = \hat{I}_{l+\frac{1}{2}}\big(\mathcal{L}^{-1}(\sigma)\big), \quad (2.2.5)$$

for the thermal average of the Stevens operators as functions of $\sigma = \sigma(T, H)$, where $c_2 = 2$, $c_4 = 8$, and $c_6 = 16$. This result has turned out to be very useful for analysing the variation of the magnetic anisotropies and the magnetoelastic strains with temperature and magnetic field. In order to take full advantage of the theory, σ in eqn (2.2.5) is usually taken as the experimental value. If this is not available, it is a better approximation to use the correct MF value for it, rather than the Langevin-function, i.e. $\sigma = B_J(x)$ where $B_J(x)$ is the Brillouin function (1.2.31), determined directly from (2.2.2), because the actual value of J has some influence on the magnitude of σ. This is particularly true for the change of σ with magnetic field. In the limit of infinite J, $\partial\sigma/\partial(JH) \simeq (1-\sigma)g\mu_B/(J^2\mathcal{J}(\mathbf{0}))$ at low temperatures, which is just a factor of three smaller than the MF value for $J = 6$, which agrees reasonably well with experiments on Tb.

The functions $\hat{I}_{l+\frac{1}{2}}(x)$, for $l = 2, 3, \cdots$ are most easily calculated from the recurrence relation

$$\hat{I}_{l+\frac{3}{2}}(x) = \hat{I}_{l-\frac{1}{2}}(x) - \frac{2l+1}{x}\hat{I}_{l+\frac{1}{2}}(x). \tag{2.2.6}$$

At low temperatures, where $x \gg 1$ and $\sigma \simeq 1-\frac{1}{x}$, it may easily be shown from (2.2.6) that $\hat{I}_{l+\frac{1}{2}}[\sigma] \simeq \sigma^{l(l+1)/2}$ (differences appear only in the third order of $m = 1-\sigma$). Hence the result (2.2.5) of the Callen–Callen theory agrees with the Zener power-law in the low-temperature limit. With increasing temperature, as x becomes comparable to 1, the exponential terms in the expansion of $\sigma \simeq 1 - \frac{1}{x} + 2\exp(-2x) + \cdots$, which have no counterpart in the classical Zener power-law, start to be important. In Chapter 5, we shall develop a detailed description of the excitations in the ferromagnet, the spin-waves. The thermal population of the spin-wave states is described by Bose statistics, assuming the availability of an infinite number of states of the single angular-momentum operators. The spin-wave theory reproduces the result of the Callen–Callen theory, in an expansion in powers of $m = 1 - \sigma$, but only if the exponential corrections above are negligible. The appearance of these terms at high temperatures signals the breakdown of the Bose approximation for the spin-wave excitations, which occurs because the actual number of states is not unlimited. As would be anticipated, this limitation in the number of states (or bandwidth if J is infinite) begins to be effective when the population of the uppermost level, which in the MF approximation is just proportional to $\exp(-2x)$, becomes significant. In the limit of a small relative magnetization, where $x \ll 1$, the Zener power-law and the spin-wave theory are both inadequate, whereas the Callen–Callen theory may still be applicable. In this limit, we may use the approximation

$$\hat{I}_{l+\frac{1}{2}}[\sigma] = \frac{3^l}{(2l+1)!!}\sigma^l \qquad ; \quad \sigma \ll 1. \tag{2.2.7}$$

One of the advantages of the Callen–Callen theory is that the results only depend on the one parameter σ, but not explicitly on the Hamiltonian. The relative magnetization may then be determined either by experiment, or by MF or more accurate theories, which result in a σ which depends on the actual Hamiltonian employed. The simplicity of this result may be impaired if the magnetic anisotropy of the system is substantial, so that the exchange interaction is no longer the dominant term in the density matrix. We shall be mostly concerned with the applicability of the theory at low temperatures, and the introduction of an axial-anisotropy term, such as $B_2^0 O_2^0(\mathbf{J}_i)$, is not inimical to the theory in this regime, provided that the magnetization is along the anisotropy c-axis, i.e. if B_2^0 is negative. Since only the lowest states are important at low temperatures and, in the MF approximation, these are still reasonably well accounted for by the density matrix in eqn (2.2.1), only the value of x is changed, with no direct consequences for the result. There are however noticeable effects if the anisotropy destroys the rotational symmetry about the magnetization axis. This is the case if B_2^0 is positive and forces the moments to lie in the basal plane, so that it requires a magnetic field to pull them out of it, whereas they may rotate much more freely within the plane, since B_6^6 is unimportant compared to the axial anisotropy. As we shall discuss in detail in Chapter 5, the ground state in this situation is no longer the fully-polarized state, the expectation value of J_z is slightly smaller than J at zero temperature, and the lower symmetry of the anisotropy field has direct consequences for the nature of the elementary spin-wave excitations, and thus for the form of the density matrix. The necessary modification of the Callen–Callen theory may be developed in two ways. One is to analyse the influence of the anisotropy on the low-temperature elementary excitations, and thereby derive the density matrix, as is done in Chapter 5. The other approach is numerical and involves the construction of a Hamiltonian which has the right transition temperature and the correct anisotropy fields, in the MF approximation. ρ_{MF} may then be calculated as a function of temperature, and results corresponding to (2.2.5), relating the expectation values of the various Stevens operators to the relative magnetization, may be obtained numerically. By the same argumentation as that used by Callen and Shtrikman (1965), these results may be expected to be insensitive to the actual model Hamiltonian used for describing the system. In the low temperature limit, the spin-wave theory supports this point of view, as its results are described in terms of only two parameters. One is the relative magnetization σ, as before, while the other, $\widetilde{b}$ or $\eta_{\pm} = (1 \pm \widetilde{b})(1 - \frac{1}{2}\widetilde{b}^2)$, measures the eccentricity of the anisotropic potential about the axis of magnetization.

In our discussion of the Callen–Callen theory, we have assumed

that the quantization axis (z-axis), defining the Stevens operators, coincides with the direction of magnetization. We shall continue to use this convention, but must then take account of the difficulty that the crystal-field Hamiltonian in the hcp metals only has the simple form of eqn (1.4.6b) if the quantization axis is chosen to be along the c- or ζ-direction. In order to distinguish between the two systems, we shall denote the Stevens operators in the Hamiltonian defined with respect to the crystallographic axes, i.e. in the (ξ, η, ζ)-coordinate system, by $Q_l^m(\mathbf{J})$. The direction of magnetization, the z-axis, is specified by the polar angles (θ, ϕ) in the (ξ, η, ζ)-coordinate system, and we must introduce the following transformation of the angular momentum operators in $Q_l^m(\mathbf{J})$:

$$\begin{aligned} J_\xi &= J_z \sin\theta\cos\phi - J_x \cos\theta\cos\phi + J_y \sin\phi \\ J_\eta &= J_z \sin\theta\sin\phi - J_x \cos\theta\sin\phi - J_y \cos\phi \\ J_\zeta &= J_z \cos\theta + J_x \sin\theta, \end{aligned} \tag{2.2.8}$$

choosing the y-axis to lie in the basal-plane. By this transformation, Q_l^m is expressed as a linear combination of the Stevens operators $O_l^{m'}$, with the same l but various m'-values. For instance, we have

$$\begin{aligned} Q_2^0 &= 3J_\zeta^2 - J(J+1) \\ &= 3J_z^2\cos^2\theta + 3J_x^2\sin^2\theta + \tfrac{3}{2}(J_zJ_x + J_xJ_z)\sin 2\theta - J(J+1) \\ &= \tfrac{1}{2}O_2^0(3\cos^2\theta - 1) + \tfrac{3}{2}O_2^2\sin^2\theta + 3O_2^1\sin 2\theta. \end{aligned} \tag{2.2.9}$$

Carrying out the same transformation on Q_2^2 we find the following relations:

$$\begin{aligned} Q_2^0 &= \tfrac{1}{2}(-O_2^0 + 3O_2^2) \\ Q_2^2 &= \tfrac{1}{2}(O_2^0 + O_2^2) \qquad ; \quad \phi = p\pi, \end{aligned} \tag{2.2.10}$$

when the moment is in the basal-plane ($\theta = \pi/2$). The expectation value of Q_2^2 is relevant for determining the γ-strain $\epsilon_{\gamma 1}$, as shown in (1.5.29). According to the result (2.2.5) of Callen and Callen, $\langle O_2^2\rangle$ should vanish, but in a basal-plane ferromagnet this may not occur. The eccentricity parameter mentioned above is just defined as

$$\widetilde{b} = \langle O_2^2\rangle / \langle O_2^0\rangle, \tag{2.2.11}$$

which is zero, by definition, only if the anisotropy is invariant with respect to a rotation about the z-axis.

The numerical programme sketched above has been carried through for a model corresponding to Tb. The effective basal-plane anisotropy is about a factor of 10 smaller than the axial anisotropy, so that $\widetilde{b}$ is

about -0.03 at zero temperature. The negative sign of $\widetilde{b}$ shows that the fluctuations of the moments within the plane are larger than those out of the plane, as measured respectively by $\langle J_y^2 \rangle$ and $\langle J_x^2 \rangle$, since $O_2^2 = J_x^2 - J_y^2$. In Fig. 2.2 the numerical results for $\langle O_2^0 \pm O_2^2 \rangle / J^{(2)}$ are compared with the predictions of the Callen–Callen theory, and of the linear spin-wave theory developed in Chapter 5, in which the MF values (5.3.23) of m_o and b_o are used, instead of (5.3.18). The Callen–Callen theory predicts that both thermal averages vary like $\hat{I}_{5/2}(\sigma)$, which is not consistent with a $\widetilde{b}$ different from zero. Furthermore, the effective power-laws in the zero-temperature limit are changed from σ^3 to $\langle O_2^0 - O_2^2 \rangle \propto \sigma^{2.65}$, and $\langle O_2^0 + O_2^2 \rangle \propto \sigma^{3.3}$. The predictions of the spin-wave theory are consistent with the numerical results at low temperatures, both with respect to the absolute magnitude of the expectation values and to the effective power-laws, and it appears to give a reasonably correct description of

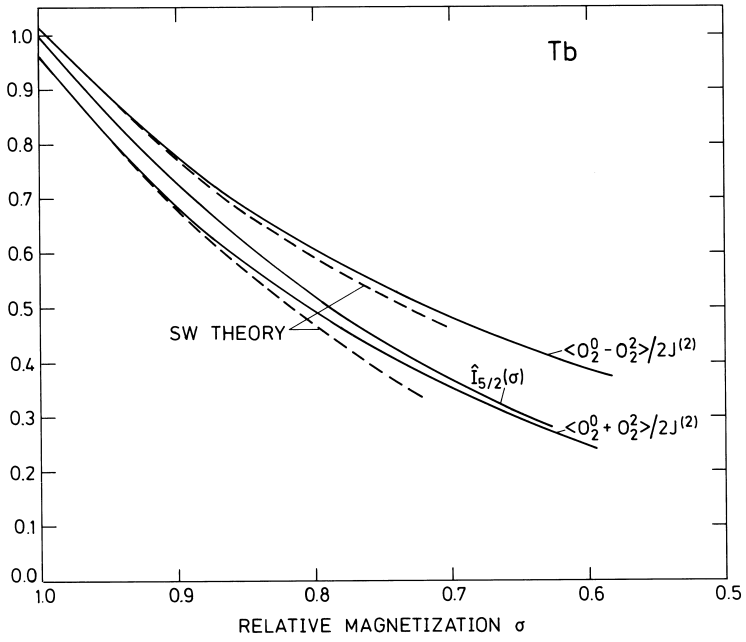

Fig. 2.2. Calculations of the dependence of the expectation values of the Stevens operators $\langle O_2^0 \pm O_2^2 \rangle$ on the relative magnetization in Tb. The numerical calculations described in the text differ from the Callen–Callen result $\hat{I}_{5/2}(\sigma)$, but agree at low temperatures with the predictions of spin-wave theory.

the system as long as σ is greater than about 0.8. The same picture holds true for other combinations of Stevens operators, but the discrepancies between the different theories are accentuated as the rank increases. Figure 2.3 shows the example of $\langle Q_6^6 \rangle$. The absolute magnitude of this quantity is reduced by nearly 40% in the zero-temperature limit, as compared with the Callen–Callen theory, and the slope of the numerical calculation, in the semi-logarithmic plot, changes with σ, leading to an effective power-law depending on the interval over which it is measured. In the zero-temperature limit, $\langle Q_6^6 \rangle$ is proportional to approximately σ^{26}, instead of the Callen–Callen result σ^{21}.

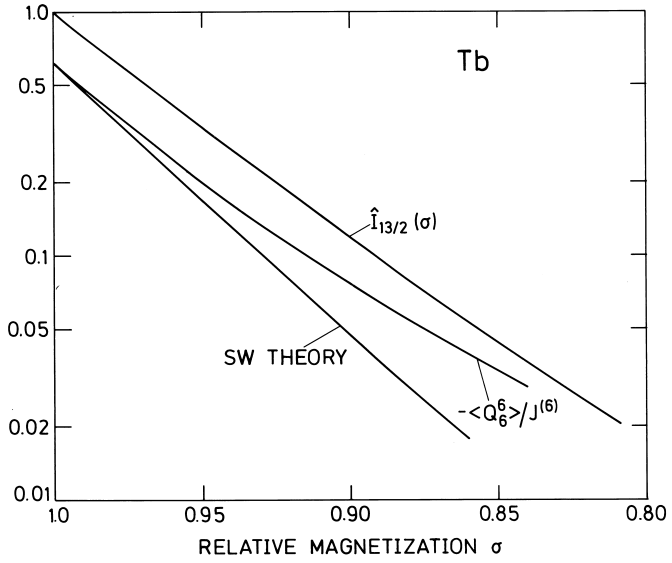

Fig. 2.3. The dependence on the relative magnetization of the expectation value of the Stevens operator $\langle Q_6^6 \rangle$, which determines the hexagonal magnetic anisotropy, in Tb. The numerical calculations and the spin-wave theory both predict a large reduction in this quantity at low temperatures, compared with the Callen–Callen theory.

The numerical results are expected to be sensitive to the magnitude of the anisotropy, rather than to the actual parameters which determine the anisotropy, and the spin-wave theory indicates that this expectation is fulfilled, at least at low temperatures. However, in order to obtain the right variation of the anisotropy fields with temperature, i.e. of $\widetilde{b}$ compared to σ, it is necessary to select appropriate linear combinations of Stevens operators of various ranks for the modelling of the different anisotropy terms. At high temperatures, for instance, $\widetilde{b}$ is determined

by the low-rank terms alone, i.e. by B_2^0 if anisotropic dipole–dipole coupling is neglected. Using $\beta = (k_B T)^{-1}$ as an expansion parameter, and assuming the magnetization to lie in the basal plane, we find, to leading order in the crystal-field parameters introduced in eqn (1.4.6*b*),

$$\langle Q_2^2 \rangle = \tfrac{3}{5} J^{(2)} \sigma^2 \frac{J + \frac{3}{2}}{J+1} \simeq J^{(2)} \hat{I}_{5/2}[\sigma], \tag{2.2.12a}$$

using (2.2.7) and neglecting the small $1/J$ corrections, whereas

$$\langle Q_2^0 \rangle = -\langle Q_2^2 \rangle - \tfrac{4}{5} J^{(2)} (J+1)(J+\tfrac{3}{2}) \beta B_2^0, \tag{2.2.12b}$$

which depends on the anisotropy, but only on the term of lowest rank. Considering the *field* dependence of the two expectation values, as determined by their dependence on σ, we observe that the Callen–Callen theory leads to the right result in this high-temperature limit. The two relations above explain the behaviour of $\langle O_2^0 \pm O_2^2 \rangle$ in Fig. 2.2, when σ becomes small, as $\langle O_2^0 + O_2^2 \rangle / 2J^{(2)}$ should approach $\hat{I}_{5/2}(\sigma)$ at small values of σ, and go to zero at the transition temperature. $\langle O_2^0 - O_2^2 \rangle / 2J^{(2)}$, on the other hand, should still be non-zero (about 0.23 as determined by $T_N \simeq 229\,\mathrm{K}$ and the value $B_2^0 = 0.18\,\mathrm{meV}$ used in the model) when T_N is approached from below and σ vanishes.

2.2.2 Anisotropic contributions to the free energy

The anisotropy of a magnetic system is determined by those contributions to the free energy which depend on the polar angles (θ, ϕ), which specify locally the direction of the moments. Restricting ourselves to the case of a ferromagnet in a uniform field, we may expand the free energy in terms of functions proportional to the spherical harmonics, as in eqn (1.5.22). To relate this expansion to the Hamiltonian (2.1.1), we may use (2.1.5), which states that any change in the free energy due to a change of the angles is given by $\delta \tilde{F} = \langle \delta \mathcal{H} \rangle$. The field is the independent variable in $\tilde{F}$ but, as in (2.1.22), we wish the magnetization to be the independent variable. To obtain this free energy $F(\theta, \phi)$, we subtract the Zeeman energy, so that $F(\theta, \phi) = \tilde{F} - \langle \mathcal{H}_\mathrm{Z} \rangle$, where the field needed for establishing the specified angles is determined from the equilibrium condition $\delta \tilde{F} = 0$. In the ferromagnet, the moments all point in the same direction, and any contributions from the isotropic-exchange coupling cancel out in $\delta \mathcal{H}$. The free-energy function $F(\theta, \phi)$ is thus determined by

$$\delta F(\theta, \phi) = \big\langle \delta(\mathcal{H}_\mathrm{cf} + \mathcal{H}_\mathrm{Z}) \big\rangle - \delta \big\langle \mathcal{H}_\mathrm{Z} \big\rangle. \tag{2.2.13}$$

Introducing the angle variables in the Hamiltonian by the transformation (2.2.8), we find that the operators of rank l become angle-dependent

linear combinations of the l-rank Stevens operators, which have their polar axis along the z-axis defined by the direction of the moments. The variational expression for the free energy then involves the calculation of the expectation values of these Stevens operators. To leading order in the crystal-field parameters, we may neglect the influence of the anisotropy terms on the thermal averages in (2.2.13). This is the approximation used by Callen and Callen, and we may utilize their result, eqn (2.2.5). This has the consequence that, in the various linear combinations of Stevens operators, only those terms in which $m = 0$ contribute to the free energy, to leading order in the anisotropy parameters. From the expansion (2.2.9) of Q_2^0, we find the following result:

$$\langle \delta(Q_2^0) \rangle \simeq \langle O_2^0 \rangle \delta\{ \tfrac{1}{2}(3\cos^2\theta - 1) \}$$

and, repeating this calculation for the other operators, we have in general

$$\langle \delta(Q_l^0) \rangle \simeq \langle O_l^0 \rangle \delta P_l(\cos\theta) \quad ; \quad \langle \delta(Q_6^6) \rangle \simeq \tfrac{1}{16} \langle O_6^0 \rangle \delta\{ \sin^6\theta \cos 6\phi \}. \tag{2.2.14}$$

Because $\langle J_x \rangle = \langle J_y \rangle = 0$, the Zeeman terms in (2.2.13) cancel within this approximation, and an integration of $\delta F(\theta, \phi)$ leads to

$$F(\theta,\phi)/N \simeq f_0 + \sum_l B_l^0 \langle O_l^0 \rangle P_l(\cos\theta) + \tfrac{1}{16} B_6^6 \langle O_6^0 \rangle \sin^6\theta \cos 6\phi. \tag{2.2.15}$$

Comparing this result with the free energy expression (1.5.22), and introducing the anisotropy parameters $\kappa_l^m(T)$, we obtain to a first approximation

$$\kappa_l^0(T) = c_l B_l^0 J^{(l)} \hat{I}_{l+\frac{1}{2}}[\sigma] \qquad ; \quad \kappa_6^6(T) = B_6^6 J^{(6)} \hat{I}_{13/2}[\sigma], \tag{2.2.16}$$

with $\sigma = \sigma(T)$, which leads to eqn (1.5.24) at zero temperature ($\sigma = 1$).

The equilibrium values of the angles in zero field are determined by $\partial F(\theta,\phi)/\partial\theta = \partial F(\theta,\phi)/\partial\phi = 0$. In the above result for the free energy, the ϕ-dependence is determined exclusively by B_6^6, the sign of which then determines whether the a- or b-directions are the magnetically easy or hard axes in the basal-plane ($\phi_0 = p\pi/3$ or $\pi/2 + p\pi/3$). Because B_6^6 is a sixth-rank coupling parameter, the importance of this anisotropy decreases rapidly with the magnetization; $\hat{I}_{13/2}[\sigma] \propto \sigma^{21}$ at low temperatures, or σ^6 when σ is small. The axial anisotropy derives from all four parameters, and the equilibrium value θ_0 is determined by minimizing

$$\begin{aligned} f(u = \cos\theta) &= F(\theta,\phi_0)/N - f_0 \\ &= \tfrac{1}{2}\kappa_2^0(3u^2 - 1) + \tfrac{1}{8}\kappa_4^0(35u^4 - 30u^2 + 3) \\ &\quad + \tfrac{1}{16}\kappa_6^0(231u^6 - 315u^4 + 105u^2 - 5) - |\kappa_6^6|(1 - u^2)^3. \end{aligned} \tag{2.2.17}$$

Equation (2.2.16) shows that the various anisotropy parameters depend differently on temperature. At high temperatures, κ_2^0 dominates and its sign determines whether the moments are parallel or perpendicular to the c-axis. As the temperature is decreased, the importance of the higher-rank terms grows, putting increasing weight on the terms of fourth and sixth power in $\cos\theta$. The equilibrium value $\theta_0(T)$ of θ may therefore change as a function of temperature, as occurs in Ho and Er, and also in Gd where, however, the theory of this section is not immediately applicable.

The coefficients in the expansion for the free energy may be obtained from experimental studies of the magnetization as a function of the magnitude and direction of an applied magnetic field. The axial part of the anisotropy is predominantly determined by the three κ_l^0-parameters, and it is not usually easy to separate their contributions. At low temperatures, where the higher-rank terms become relatively important, the axial anisotropy in the heavy rare earths is frequently so strong that it is only possible to change θ by a few degrees from its equilibrium value. Under these circumstances, it is only possible to measure the components of the susceptibility, allowing a determination of the second derivatives of $F(\theta,\phi)$ in the equilibrium state $(\theta,\phi)=(\theta_0,\phi_0)$. The x-axis lies in the symmetry z–ζ plane and the transverse part of the susceptibility tensor is diagonal with respect to the (x,y)-axes. With a field h_x applied in the x-direction, the moments rotate through an angle $\delta\theta=\theta-\theta_0$, giving a component $\langle J_x\rangle=-\langle J_z\rangle\delta\theta=\chi_{xx}h_x$. Introducing the notation $F_{\theta\theta}\equiv\partial^2F(\theta,\phi)/\partial\theta^2$ at $(\theta,\phi)=(\theta_0,\phi_0)$, and similarly for the other second derivatives, we may write

$$F=F(\theta_0,\phi_0)+\tfrac{1}{2}F_{\theta\theta}(\delta\theta)^2+\tfrac{1}{2}F_{\phi\phi}(\delta\phi)^2+N\langle J_z\rangle\delta\theta h_x,$$

in the limit where the field goes to zero. The term $F_{\theta\phi}=0$, because $\sin 6\phi_0=0$. At equilibrium, $\delta\theta=-N\langle J_z\rangle h_x/F_{\theta\theta}$, which determines the susceptibility. When the field is applied in the y-direction, i.e. along the direction $(-\sin\phi_0,\cos\phi_0,0)$, the Zeeman contribution to F is

$$N\langle J_z\rangle h_y\sin\theta\sin(\phi-\phi_0)=N\langle J_z\rangle h_y\sin\theta_0\delta\phi,$$

with $\langle J_y\rangle=-\langle J_z\rangle\sin\theta_0\delta\phi=\chi_{yy}h_y$. Minimizing the free energy in the presence of a field along the y-axis, we may derive the other susceptibility component, obtaining

$$\chi_{xx}=N\langle J_z\rangle^2/F_{\theta\theta}\qquad;\quad\chi_{yy}=N\langle J_z\rangle^2\sin^2\theta_0/F_{\phi\phi}. \tag{2.2.18}$$

In calculating χ_{yy}, we have assumed that $\theta_0\neq 0$; if $\theta_0=0$ then $\chi_{yy}=\chi_{xx}$. Equation (2.2.18) is also valid in the presence of an external field, provided that the effects due to the Zeeman contribution,

$F_Z = -Ng\mu_B \mathbf{H}\cdot\langle\mathbf{J}\rangle$, are included explicitly in $F(\theta_0,\phi_0)$ and its derivatives. Introducing the expression (2.2.17) for the free energy, in the two cases where the moments are either parallel or perpendicular to the c-axis, we find

$$1/\chi_{xx} = 1/\chi_{yy} = -(3\kappa_2^0+10\kappa_4^0+21\kappa_6^0)/(\sigma J)^2 \qquad ; \quad \theta_0 = 0, \quad (2.2.19a)$$

or

$$\begin{aligned} 1/\chi_{xx} &= (3\kappa_2^0 - \tfrac{15}{2}\kappa_4^0 + \tfrac{105}{8}\kappa_6^0 + 6|\kappa_6^6|)/(\sigma J)^2 \\ 1/\chi_{yy} &= 36|\kappa_6^6|/(\sigma J)^2 \end{aligned} \qquad ; \quad \theta_0 = \frac{\pi}{2}, \qquad (2.2.19b)$$

which must be positive if the structure is to be stable. In order to determine the higher derivatives of the free energy, a transverse field greater than that corresponding to the linear regime described by the (zero-field) susceptibility must be applied. The application of a large magnetic field perpendicular to the magnetization axis, in a strongly anisotropic system, creates a large mechanical torque, which may cause practical problems with maintaining the orientation of the crystal. If the experimental facilities do not allow the determination of the higher derivatives, the different temperature dependences of the various anisotropy parameters may yield a rough separation of their contributions to the total axial anisotropy. However the Callen–Callen theory is an approximation, the corrections to which are important if the anisotropy is large, and there are other contributions to the free energy than those which we have considered above.

The results derived above are only valid if the anisotropy energies are small compared to the exchange energy. In order to demonstrate the kind of modifications which may appear in higher order, we shall consider the simplest possible case, where only B_2^0 is non-zero, and we shall only calculate the free energy at zero temperature in the MF approximation, i.e. the ground-state energy of a single site subjected to the exchange field $h_{\rm ex} = \langle J_z\rangle\mathcal{J}(\mathbf{0})$, with $\langle J_z\rangle = \sigma J$. In this case, the MF Hamiltonian (2.1.16) is

$$\begin{aligned} \mathcal{H} &= -(J_z - \tfrac{1}{2}\sigma J)\sigma J\mathcal{J}(\mathbf{0}) - h(J_z\cos\theta + J_x\sin\theta) \\ &+ B_2^0\big[3J_z^2\cos^2\theta + 3J_x^2\sin^2\theta + \tfrac{3}{2}(J_zJ_x + J_xJ_z)\sin 2\theta - J(J+1)\big], \end{aligned} \qquad (2.2.20)$$

in an applied field h along the ζ-axis. With the J_z-eigenstates as the basis, the leading-order ground-state energy is

$$E_0^0 = <J\,|\,\mathcal{H}\,|\,J> = -(1-\tfrac{1}{2}\sigma)\sigma J^2\mathcal{J}(\mathbf{0}) - hJ\cos\theta + B_2^0 J^{(2)}(3\cos^2\theta - 1).$$

The off-diagonal matrix elements involving the ground state are

$$<J-1\,|\,\mathcal{H}\,|\,J> = \big\{6(J-\tfrac{1}{2})B_2^0\cos\theta - h\big\}(J/2)^{1/2}\sin\theta$$
$$<J-2\,|\,\mathcal{H}\,|\,J> = \tfrac{3}{2}\{2J^{(2)}\}^{1/2}B_2^0\sin^2\theta.$$

We shall only be concerned with terms up to second order in B_2^0 and h, so that we may use second-order perturbation theory, and it is sufficiently accurate to approximate the energy differences between the ground state and the first and second excited-states by respectively $\Delta_1 = J\mathcal{J}(\mathbf{0})$ and $\Delta_2 = 2J\mathcal{J}(\mathbf{0})$. Because of the mixing of the states, $\sigma = \langle J_z\rangle/J = 1-m$ becomes slightly smaller than 1, but this only affects the exchange contribution quadratic in m, as $(1-\frac{1}{2}\sigma)\sigma = \frac{1}{2}(1-m^2)$. To second order, the ground-state energy is found to be

$$E_0(h) = -\tfrac{1}{2}J^2\mathcal{J}(\mathbf{0}) - hJ\cos\theta + B_2^0J^{(2)}(3\cos^2\theta - 1)$$
$$-\tfrac{1}{2}\big\{6(J-\tfrac{1}{2})B_2^0\cos\theta - h\big\}^2\sin^2\theta/\mathcal{J}(\mathbf{0}) - \tfrac{9}{4}(J-\tfrac{1}{2})(B_2^0)^2\sin^4\theta/\mathcal{J}(\mathbf{0}). \tag{2.2.21}$$

The minimum condition $\partial E_0/\partial\theta = 0$ leads to

$$h = h_0 = 6(J-\tfrac{1}{2})B_2^0\big[1 + 3B_2^0\sin^2\theta/\{2J\mathcal{J}(\mathbf{0})\}\big]\cos\theta \qquad \text{or} \quad \sin\theta = 0,$$

to second order in B_2^0. The free energy $F(\theta,\phi)$ at zero temperature is then, in both cases,

$$F(\theta,\phi)/N = E_0(h_0) + h_0J\sigma\cos\theta$$
$$= -\tfrac{1}{2}J^2\mathcal{J}(\mathbf{0}) + \tfrac{1}{2}\tilde{\kappa}_2^0(3\cos^2\theta - 1) + \tfrac{3}{4}b\tilde{\kappa}_2^0\sin^4\theta,$$

with

$$\tilde{\kappa}_2^0 = 2B_2^0J^{(2)} \qquad ; \quad b = -3B_2^0/\{2J\mathcal{J}(\mathbf{0})\}, \tag{2.2.22a}$$

and the relative magnetization is $\sigma = 1 - (J-\frac{1}{2})b^2\sin^4\theta$. The b-parameter introduced here is the leading order contribution to $\widetilde{b}$, defined in (2.2.11), when $\theta = \pi/2$. One important feature illustrated by this calculation is that the O_2^m-term in Q_2^0, with m odd, is cancelled by the Zeeman contribution, to second order in B_2^0. This is a consequence of the freedom to replace the equilibrium condition $\partial F/\partial\theta = 0$ by the requirement that $\langle J_x\rangle$ (and $\langle J_y\rangle$) should vanish, by definition, with the implication that the matrix-element $<J-1\,|\,\mathcal{H}\,|\,J>$ must be zero within the present approximation. Bowden (1977) did not take the Zeeman effect into account, and therefore obtained an erroneously strong renormalization of the anisotropy. The second derivatives of $F(\theta,\phi)$ are $F_{\phi\phi} = 0$, and

$$F_{\theta\theta}/N = -3\tilde{\kappa}_2^0(1 - b\sin^2\theta)\cos 2\theta + \tfrac{3}{2}\tilde{\kappa}_2^0b\sin^2 2\theta. \tag{2.2.22b}$$

There is no change in the axial susceptibility in the axial ferromagnet, for which $\theta = 0$, but the higher derivatives are affected by the modifications $\kappa_2^0(0) = \tilde{\kappa}_2^0(1 - \frac{4}{7}b)$ and $\kappa_4^0(0) = \frac{6}{35}b\tilde{\kappa}_2^0$. The correction to the Callen–Callen theory is proportional to b, which is of the order $1/J$ times the ratio between the anisotropy and the exchange energy ($\propto B_2^0 J^{(2)}/J^2\mathcal{J}(\mathbf{0})$), and hence becomes smaller for larger values of J. This calculation may be extended to higher order and to non-zero temperatures, but the complications are much reduced by the application of the *Holstein–Primakoff transformation* which utilizes directly the factor $1/J$ in the expansion, as we shall see in the discussion of the spin-wave theory in Chapter 5.

In the ferromagnetic phase, the ordered moments may distort the lattice, due to the magnetoelastic couplings, and this gives rise to additional contributions to $F(\theta,\phi)$. We shall first consider the effects of the γ-strains by including the magnetoelastic Hamiltonian, incorporating (1.4.8) and (1.4.11),

$$\begin{aligned}\mathcal{H}_\gamma = \sum_i \big[\tfrac{1}{2}c_\gamma(\epsilon_{\gamma 1}^2 + \epsilon_{\gamma 2}^2) - B_{\gamma 2}\big\{Q_2^2(\mathbf{J}_i)\epsilon_{\gamma 1} + Q_2^{-2}(\mathbf{J}_i)\epsilon_{\gamma 2}\big\} \\ - B_{\gamma 4}\big\{Q_4^4(\mathbf{J}_i)\epsilon_{\gamma 1} - Q_4^{-4}(\mathbf{J}_i)\epsilon_{\gamma 2}\big\}\big],\end{aligned} \tag{2.2.23}$$

retaining only the lowest-rank couplings ($l = 2$ and 4 of respectively the $\gamma 2$ and $\gamma 4$ terms). The equilibrium condition

$$\partial F/\partial\epsilon_{\gamma 1} = \big\langle \partial\mathcal{H}_\gamma/\partial\epsilon_{\gamma 1}\big\rangle = 0, \tag{2.2.24}$$

and similarly for $\epsilon_{\gamma 2}$, leads to the equilibrium strains

$$\begin{aligned}\epsilon_{\gamma 1} &= \big(B_{\gamma 2}\langle Q_2^2\rangle + B_{\gamma 4}\langle Q_4^4\rangle\big)/c_\gamma \\ \epsilon_{\gamma 2} &= \big(B_{\gamma 2}\langle Q_2^{-2}\rangle - B_{\gamma 4}\langle Q_4^{-4}\rangle\big)/c_\gamma.\end{aligned} \tag{2.2.25}$$

The conventional magnetostriction parameters C and A are introduced via the equations

$$\begin{aligned}\epsilon_{\gamma 1} &= C\sin^2\theta\cos 2\phi - \tfrac{1}{2}A\sin^4\theta\cos 4\phi \\ \epsilon_{\gamma 2} &= C\sin^2\theta\sin 2\phi + \tfrac{1}{2}A\sin^4\theta\sin 4\phi\end{aligned} \tag{2.2.26a}$$

(Mason 1954). Expressing Q_l^m in terms of O_l^m, and retaining only the terms with $m = 0$, we may derive these parameters from (2.2.25), obtaining

$$\begin{aligned}C &= \frac{1}{c_\gamma}B_{\gamma 2}J^{(2)}\hat{I}_{5/2}[\sigma] \\ A &= -\frac{2}{c_\gamma}B_{\gamma 4}J^{(4)}\hat{I}_{9/2}[\sigma].\end{aligned} \tag{2.2.26b}$$

Within this approximation, the γ-strain contribution $F_\gamma(\theta,\phi)$ to the free energy is

$$\begin{aligned} F_\gamma(\theta,\phi) &= \langle \mathcal{H}_\gamma \rangle = -\tfrac{1}{2}c_\gamma\big(\epsilon_{\gamma 1}^2 + \epsilon_{\gamma 2}^2\big)N \\ &= -\tfrac{1}{2}c_\gamma\big(C^2\sin^4\theta + \tfrac{1}{4}A^2\sin^8\theta - CA\sin^6\theta\cos 6\phi\big)N, \end{aligned} \tag{2.2.27}$$

showing that these strains affect the axial-anisotropy parameters $\kappa_l^0(T)$, introducing effects of higher rank than $l = 6$, and that the six-fold anisotropy in the basal plane is now

$$\kappa_6^6(T) = B_6^6 J^{(6)} \hat{I}_{15/2}[\sigma] + \tfrac{1}{2}c_\gamma CA. \tag{2.2.28}$$

When both C and A are non-zero, the maximum area-conserving elongation of the hexagonal planes varies between $|C + \frac{1}{2}A|$ and $|C - \frac{1}{2}A|$, which results in a ϕ-dependent magnetoelastic energy, and thus a contribution to κ_6^6. The γ-strain hexagonal anisotropy decreases more slowly (like σ^{13} at low temperatures) than the B_6^6 term, as σ decreases, and therefore dominates at sufficiently high temperatures.

The ε-strains may be included in a similar way. Retaining only the lowest-rank coupling $B_{\varepsilon 1} \equiv B_{\varepsilon 1}^{(l=2)}$ in eqn (1.4.12), we have

$$\mathcal{H}_\varepsilon = \sum_i \big[\tfrac{1}{2}c_\varepsilon(\epsilon_{\varepsilon 1}^2 + \epsilon_{\varepsilon 2}^2) - B_{\varepsilon 1}\big\{Q_2^1(\mathbf{J}_i)\epsilon_{\varepsilon 1} + Q_2^{-1}(\mathbf{J}_i)\epsilon_{\varepsilon 2}\big\}\big]. \tag{2.2.29}$$

Introducing the magnetostriction parameter H_ε of Mason (1954) (the index ε should prevent any confusion with the magnetic field) by

$$\epsilon_{\varepsilon 1} = \tfrac{1}{4}H_\varepsilon \sin 2\theta\cos\phi \qquad ; \quad \epsilon_{\varepsilon 2} = \tfrac{1}{4}H_\varepsilon \sin 2\theta \sin\phi, \tag{2.2.30a}$$

we obtain within the Callen–Callen theory

$$H_\varepsilon = \frac{2}{c_\varepsilon} B_{\varepsilon 1} J^{(2)} \hat{I}_{5/2}[\sigma], \tag{2.2.30b}$$

and the ε-strain contribution to the free energy

$$F_\varepsilon(\theta,\phi) = -\tfrac{1}{32}N c_\varepsilon H_\varepsilon^2 \sin^2 2\theta. \tag{2.2.31}$$

The α-strains (1.4.10) do not influence the symmetry of the system, but they do make a contribution, essentially proportional to $\langle Q_2^0 \rangle$, to the anisotropy, the effects of which may be derived in the same way as those of the γ- and ε-strains. The magnetoelastic contributions to the free energy can be estimated experimentally if the elastic constants are known, by a determination of the strains as a function of the magnetization. The

knowledge of the equilibrium strains may also be used for a reasonable estimate of the magnetoelastic modifications of the second derivatives, provided that the additional assumption is made that the couplings of lowest rank are dominant. For example, the higher-rank γ-strains in the basal-plane magnet make contributions to the axial anisotropy which cannot be written in terms of C and A in eqn (2.2.27). A more direct estimate of the contributions to the second derivatives requires an experimental determination of how the strains behave when the direction of the magnetization is changed. In basal-plane ferromagnets, such as Tb and Dy, it may be possible to observe the ϕ-dependence of the strains (Rhyne and Legvold 1965a), whereas if the axial anisotropy is large, it may be very difficult to determine the variation of the strains with θ. In the case of the α-strains, the argument that the $(l = 2)$ couplings are dominant is not sufficient for a determination of their effect on the axial anisotropy. The reason is that the *two-ion magnetoelastic couplings* of lowest rank, i.e. the dipolar interactions

$$\Delta\mathcal{H}^{\alpha}_{\rm me} = -\sum_{ij}\Big[\big\{D_{10}(ij)\epsilon_{\alpha 1} + D_{20}(ij)\epsilon_{\alpha 2}\big\}\,\mathbf{J}_i\cdot\mathbf{J}_j + \big\{D_{13}(ij)\epsilon_{\alpha 1} + D_{23}(ij)\epsilon_{\alpha 2}\big\}J_{i\zeta}J_{j\zeta}\Big], \tag{2.2.32}$$

may be important. This is the case in Tb and Dy, as shown by the analysis of the stress-dependence of the Néel temperatures (Bartholin *et al.* 1971). These interactions affect the α-strains, but they contribute differently to the axial anisotropy from the $(l = 2)$-terms in the single-ion magnetoelastic Hamiltonian (1.4.10).

The simplifications introduced in the above discussion of the ferromagnet may also be utilized in non-uniform systems, because the MF approximation allows the individual ions to be treated separately. However, the isotropic two-ion contributions no longer cancel in $\delta F(\theta,\phi)$ in (2.2.13), since the direction of the exchange field depends on the site considered. We consider as an example the helically ordered phase. If we neglect the bunching effect due to the hexagonal anisotropy, the axial anisotropy is independent of the site considered. Treating the ions as isolated, but subject to a constant exchange-field, we may calculate $F^{o}_{\theta\theta}$, corresponding to $1/\chi^{o}_{xx}$, and then use (2.1.19) to account for the induced exchange-field due to an applied field in the x- or c-direction, modulated with a wave-vector $\mathbf{q}$ along the c-axis. If the two-ion coupling between the moments is allowed to be anisotropic, the leading order result is

$$1/\chi_{xx}(\mathbf{q}) = \mathcal{J}_{\perp}(\mathbf{Q}) - \mathcal{J}_{\parallel}(\mathbf{q}) + \big(3\kappa^0_2 - \tfrac{15}{2}\kappa^0_4 + \tfrac{105}{8}\kappa^0_6\big)/(\sigma J)^2. \tag{2.2.33}$$

This is the anisotropy parameter which determines the plane in which the moments spiral, and it vanishes at the temperature T'_N at which

the c-axis moments begin to order. Just below T_N', the c-component is modulated with the wave-vector $\mathbf{Q}'$ at which $\mathcal{J}_\parallel(\mathbf{q})$ has its maximum, and only if $\mathbf{Q}' = \mathbf{Q}$ is the structure the tilted helix. If $\mathbf{Q}' = \mathbf{0}$, so that the c-axis moments are ferromagnetically ordered, the resulting structure is the *cone*.

The magnetoelastic contributions require special treatment when the structures are modulated, because of the limited ability of the lattice to adapt to various strain configurations, when the strains are spatially modulated. The magnetoelastic Hamiltonians considered above are only strictly valid in the uniform case, but they may be generalized to non-uniform structures by replacing the strains by their local values $\epsilon_{\alpha\beta}(i)$, at least in the limit where the wavelength of the modulation is much longer than the range of the interactions. At shorter wavelengths, the form of the magnetoelastic-interaction Hamiltonian may still be applicable, but the effective coupling parameters may depend on the wave-vector. This suggests that the above discussion may be largely unchanged if the magnetic structure is modulated, provided that we take account of the new constraints which we shall now examine. The displacement of the ith ion, $\mathbf{u}(\mathbf{R}_i) = \widetilde{\mathbf{R}}_i - \mathbf{R}_i$, from its equilibrium position $\mathbf{R}_i$ may be divided into a uniform and a non-uniform component, and the non-uniform part may be written as a linear combination of contributions from the *normal phonon modes* at various wave-vectors. It follows from this that a displacement of the ions which varies with a certain wave-vector should be describable in terms of the normal phonon modes at that particular wave-vector, in order to ensure that such a displacement is compatible with the lattice.

To be more specific, we shall consider the wave-vector to be along the c-axis in the hcp lattice. In the *double-zone representation*, which neglects the two different displacements of the hexagonal layers, there are only three normal modes; one longitudinal and two energetically-degenerate transverse modes. All three modes correspond to rigid displacements of the hexagonal layers. The γ-strains describe an elongation of these layers along a certain direction in the plane. If the γ-strains are uniform within each hexagonal layer, the magnitude or the direction of the elongation cannot be allowed to vary from one layer to the next, as this would destroy the crystal. Hence, even though $\langle Q_2^2(\mathbf{J}_i)\rangle$ in the equilibrium equation for $\epsilon_{\gamma 1}(i)$, corresponding to eqn (2.2.25), varies in a well-defined way in a helical structure with $\mathbf{Q}$ along the c-axis, $\epsilon_{\gamma 1}(i)$ is forced to stay constant. The site-dependent version of (2.2.25) is only valid when the right-hand sides are replaced by their averages with respect to any variation along the c-axis, and these averages vanish in the helix. This phenomenon was named the *lattice clamping effect* by Cooper (1967), and further discussed by Evenson and Liu (1969). One

of its consequences is that the γ-strain contributions (2.2.27) to the free energy cancel out in the helical phase. This behaviour of the γ-strains therefore enhances the tendency of the wave-vector of the helix to jump to one of the two commensurable values $Q = 0$ or $2\pi/c$, or may increase the stability of other commensurable structures which have a net moment in the basal-plane.

The only strain modes which are allowed to vary along the c-axis are those deriving from the transverse modes, which are $\epsilon_{\varepsilon 1}(i)$ and $\epsilon_{\varepsilon 2}(i)$, and the longitudinal component $\epsilon_{33}(i)$. Like the γ-strains, the α-strains $\epsilon_{11}(i)$ and $\epsilon_{22}(i)$ must remain constant. In the longitudinally polarized phase, the ε-strains are not affected by the ordered moment. The uniform α-strains are determined by the average of $Q_l^0(\mathbf{J}_i)$ and, in addition, the c-axis moments induce a non-uniform longitudinal-strain mode $\epsilon_{33}(i) \propto \langle J_{i\zeta}\rangle^2$ at the wave-vector $2\mathbf{Q}$, twice the ordering wave-vector. The amplitude $\epsilon_{2\mathbf{Q}}$, in $\epsilon_{33}(i) = \epsilon_{2\mathbf{Q}} \cos(2QR_{i\zeta})$, may be determined by the equilibrium conditions for the single sites, with the magnetoelastic-coupling parameters replaced by those corresponding to $2\mathbf{Q}$. The longitudinal strain at site i is directly related to the displacement of the ion along the ζ-axis; $\epsilon_{33}(i) = \partial u_\zeta/\partial R_{i\zeta}$ and hence $u_\zeta(\mathbf{R}_i) = (2Q)^{-1}\epsilon_{2\mathbf{Q}} \sin(2\mathbf{Q}\cdot\mathbf{R}_i)$. Below T_N', where $\langle J_{i\xi}\rangle$ becomes non-zero, the cycloidal ordering induces an $\epsilon_{\varepsilon 1}$-strain, modulated with the wave-vector $2\mathbf{Q}$. The presence of a (static) transverse phonon mode polarized along the ξ-direction corresponds to $\partial u_\xi/\partial R_{i\zeta} = \epsilon_{13}(i) + \omega_{13}(i) \neq 0$, whereas $\partial u_\zeta/\partial R_{i\xi} = \epsilon_{13}(i) - \omega_{13}(i) = 0$. Hence it is $\epsilon_{\varepsilon 1}(i) + \omega_{13}(i)$, with $\omega_{13}(i) = \epsilon_{\varepsilon 1}(i)$, which becomes non-zero, and not just $\epsilon_{13}(i) = \epsilon_{\varepsilon 1}(i)$. In these expressions, $\omega_{13}(i)$ is the antisymmetric part of the strain tensor, which in the long-wavelength limit describes a rigid rotation of the system around the η-axis. Because such a rotation, in the absence of external fields, does not change the energy in this limit, the magnetoelastic Hamiltonian may still be used for determining $\epsilon_\varepsilon(i)$. Only when the relation between the strains and the transverse displacements is considered, is it important to include the antisymmetric part. In helically-ordered systems, the γ-strains are zero, due to the clamping effect, as are the ε-strains, because the moments are perpendicular to the c-axis. Only the α-strains may be non-zero, and because $\langle Q_l^0(\mathbf{J}_i)\rangle$ are independent of the direction of the basal-plane moments, the α-strains are the same as in the ferromagnet (we neglect the possible six-fold modification due to B_α^{66} in (1.4.10)). Their contributions to the axial anisotropy (2.2.33), to be included in κ_l^0, are also the same as in the ferromagnetic case. In the basal-plane ferromagnet, the ε strains contribute to the axial anisotropy $1/\chi_{xx}$ in eqn (2.2.19b):

$$\Delta(1/\chi_{xx}) = \frac{1}{N(\sigma J)^2}\partial^2 F_\varepsilon/\partial\theta^2 = -\tfrac{1}{4}c_\varepsilon H_\varepsilon^2/(\sigma J)^2 \quad ; \quad \theta_0 = \frac{\pi}{2}, \quad (2.2.34)$$

as derived from (2.2.31). It is straightforward to see that we get the equivalent contribution in the helix at $\mathbf{q} = \mathbf{0}$ in eqn (2.2.33), except that the coupling parameters in (2.2.34) should have the effective values at the wave-vector $\mathbf{Q}$. In the conical phase, both $\epsilon_{\varepsilon 1}(i)$ and $\epsilon_{\varepsilon 2}(i)$ become non-zero, 90° out of phase with each other, corresponding to a transverse displacement of the planes, in a direction which follows the orientation of the moments in the basal plane.

2.3 Magnetic structures of the elements

As we have seen, the 'exotic spin configurations' first observed by Koehler and his colleagues in the heavy rare earths may be understood as the result of a compromise between the competing magnetic interactions to which the moments are subjected. The complex changes which occur as the temperature is varied stem primarily from the temperature dependence of the expectation values of the terms in the MF Hamiltonian (2.1.16). The *crystal-field parameters* B_l^m are expected to change little with temperature but, as shown in the previous section, the variation of the expectation values $\langle O_l^m \rangle$ of the *Stevens operators* may give rise to a very pronounced temperature dependence of the anisotropy forces, including the magnetoelastic effects. The contribution from the *two-ion coupling* generally varies more slowly, since the exchange field is proportional to $\langle \mathbf{J}_j \rangle$ or σ, but changes in the magnitude and orientation of the ordered moments alter the band structure of the conduction electrons, which in turn modifies the *indirect exchange* $\mathcal{J}(ij)$. Hence the Fourier transform $\mathcal{J}(\mathbf{q})$, and in particular the value $\mathbf{Q}$ at which it attains its maximum, may change with temperature in the ordered phase. In addition, the possibility that *anisotropic two-ion coupling* may be of importance implies that the effective parameters of the simple MF Hamiltonian (2.1.16) may all depend on the magnitude and orientation of the moments.

The anisotropy forces favour a set of crystallographic directions, related by a rotational symmetry operator, along which the moments tend to align themselves. In particular, the low-order crystal-field term $B_2^0 \langle O_2^0(\mathbf{J}) \rangle$ gives rise to an *axial anisotropy*, which strives to confine the magnetization either to the basal plane or along the c-axis, and declines relatively slowly with temperature. Except for Gd, the rare earth elements all have a $\mathcal{J}(\mathbf{q})$ with a maximum at $\mathbf{Q} \neq \mathbf{0}$, reflecting the complexities of the Fermi surface and corresponding to a periodicity which is not generally commensurable with the lattice. Transverse and longitudinal magnetic structures can accomodate both the anisotropy and the periodicity constraints at high temperatures, with respectively uniform helical or longitudinal-wave configurations of the moments, characterized by a single wave-vector. As the temperature is lowered, however,

conditions develop which favour commensurable structures, including the ferromagnet. The *hexagonal anisotropy* distorts the helical structure, while the development of higher harmonics, assisted by the axial-anisotropy forces, favours commensurability in the longitudinal structure. The *higher-order axial-anisotropy terms* may also tend to pull the moments away from their planar or axial orientations. The application of a *magnetic field* requires further compromises, until it is so great that it coerces all the moments into alignment.

The variation of temperature and field thus reveals a rich variety of intermediate phase transitions to different structures. Most of these transitions are discontinuous, but occasionally a second-order transition is observed. In the following, we will discuss the relation between the *interactions*, and their variation, and the *magnetic structures* in the rare earths. We shall give a summary of the rather complete understanding which has been attained of the heavy elements, followed by a brief discussion of the complex structures of Nd, which is the only light rare earth which has been studied in comparable detail. The effect of a magnetic field will be exemplified by a description of the magnetization of Ho. Finally we will consider the new features which emerge when one dimension of the magnetic lattice is bounded, illustrated by some of the results from the rapidly developing study of thin films and superlattices.

2.3.1 Bulk magnetic structures

The manner in which the competing interactions express themselves is very well illustrated by the heavy hcp rare earths. In their magnetically ordered phases, all the moments in a particular plane normal to the c-axis are aligned, but their relative orientations may change from plane to plane. Fig. 1.19 illustrates some of the simpler of these structures, while the transition temperatures T_N and T_C to ordered states, respectively without and with a net moment, are given in Table 1.6.

Gd is magnetically by far the simplest of the rare earths. The exchange favours ferromagnetism and the $4f$ charge-cloud is spherically symmetric, so that the crystal-field interactions (1.4.4) are zero. However there is a residual magnetic anisotropy, which causes the moments to point preferentially along the c-axis just below T_C. At lower temperatures, the easy axis begins to deviate towards the basal plane, reaching a maximum tilt angle of 60° at 180 K before decreasing to just below 30° at 4.2 K (Corner and Tanner 1976). The anisotropy parameters are typically two or three orders of magnitude smaller than those of the other heavy rare earths (Mishima *et al.* 1976). Since the c/a ratio of Table 1.2 is less than the ideal value, the dipolar coupling induces an anisotropy, discussed in Section 5.5.1, which tends to hold the moments along the c-direction and has roughly the observed magnitude (Brooks and Good-

ings 1968). There is in addition a competing anisotropy, which has its origin in the spin–orbit coupling (1.2.13) of the conduction electron gas, which restricts the free rotation of the spins relative to the lattice. The indirect-exchange interaction then ensures that the localized spins are correspondingly constrained. The magnitude of this effect could in principle be calculated from the electronic structure, at least at absolute zero, but no serious attempts have yet been made to do so.

The small anisotropy of Gd leads to an unusual sequence of structures when it is diluted with Y. The latter has a very strong tendency to impose a periodic magnetic structure on dissolved rare earth moments (Rainford *et al.* 1988a; Caudron *et al.* 1990) and, in a concentration above about 30% in Gd, induces a helical structure below T_N. The magnetic behaviour of these alloys is completely dominated by the exchange, and the transition to the ferromagnetic structure, both with increasing Gd concentration and, as occurs if the Y concentration is not too high, with decreasing temperature, takes place by a continuous reduction of the turn angle of the helix (Palmer *et al.* 1986), as the peak in $\mathcal{J}(\mathbf{q})$ moves smoothly to the origin. At higher Y concentrations, a longitudinal wave is also formed along the c-axis, over a temperature range and with a wave-vector which are different from those of the helix. As discussed in Section 2.1.5, this behaviour shows explicitly that the exchange must be anisotropic. Furthermore, at Y concentrations just above the critical value for the formation of a helix, a ferromagnetic structure, with the easy direction along the c-axis, forms at T_C, is transformed into a basal-plane helix through a first-order transition at a lower temperature T_N, and at an even lower temperature transforms back into the aforementioned ferromagnetic structure, with the moments canted away from the c-direction.

Tb and Dy both have large axial anisotropies which confine the moments to their basal planes, and the peaks in $\mathcal{J}(\mathbf{q})$, illustrated in Fig. 1.17, induce helical structures at the respective Néel temperatures. In Tb, this peak is very small, and the spin-wave measurements illustrated in Fig. 6.1 indicate that it becomes even smaller as the helical phase is established and the superzone energy-gaps grow. Simultaneously, the (negative) anisotropy energy in the ferromagnetic phase increases, particularly the cylindrically-symmetric magnetoelastic term proportional to C^2 in (2.2.27), which makes no contribution in the helical phase because of lattice clamping. Consequently, this anisotropy energy overwhelms the exchange-energy difference (1.5.35) only ten degrees below T_N, and a first-order transition occurs to a ferromagnetic structure. The peak in the exchange function in Dy is more robust, and the helical phase correspondingly more stable but, as we have discussed in Section 1.5, a ferromagnetic transition ultimately takes place at 85 K.

An instructive example of competing anisotropy forces has been observed in a $Tb_{0.5}Dy_{0.5}$ crystal (Spano *et al.* 1988). This alloy, as would be anticipated, forms a helical structure at 206 K, and transforms into a ferromagnet at 152 K. At this temperature, the predominant anisotropy is due to the Tb magnetoelastic forces in (2.2.28), since the coefficient A is almost zero for Dy (Martin and Rhyne 1977), and the hexagonal crystal-field anisotropy for both types of ion has renormalized to a very small value. Consequently, the easy axis of magnetization is the b-axis, as in pure Tb. As the temperature is further reduced, however, the crystal-field contribution grows, roughly as σ^{21}, and since it is much greater for Dy than Tb, the easy axis switches at about 100 K to the a-direction, as in pure Dy.

Table 2.1. Crystal-field parameters (meV).

	B_2^0	B_4^0	B_6^0	B_6^6
Ho	0.024	0.0	$-9.6{\cdot}10^{-7}$	$9.2{\cdot}10^{-6}$
Er	-0.027	$-0.3{\cdot}10^{-4}$	$1.3{\cdot}10^{-6}$	$-9.0{\cdot}10^{-6}$
Tm	-0.096	0.0	$-9.2{\cdot}10^{-6}$	$8.9{\cdot}10^{-5}$

Compared with these relatively straightforward systems, the behaviour of the remainder of the magnetic heavy rare earth series, Ho, Er, and Tm, is more intriguing. As illustrated in Fig. 1.17, the peaks in $\mathcal{J}(\mathbf{q})$ are large, so that periodic structures are stabilized down to low temperatures. The crystal-field anisotropy also allows the moments to move out of the plane. In Table 2.1 are given the anisotropy parameters deduced from studies of the magnetic structures and excitations. Although these must to some extent be considered as effective values, subsuming for example the effects of two-ion and magnetoelastic anisotropy, they are among the best estimates which we have for the crystal fields in the rare earths, and they correlate well with the Stevens factors of Table 1.4.

Ho demonstrates the interplay of the various interactions in an exemplary manner. The positive value of B_2^0 and the peak in the exchange function again stabilize the helix at T_N. The peak value $\mathcal{J}(\mathbf{Q})$ is now so large, however, that the cylindrically-symmetric magnetoelastic energy, which is substantially smaller than that of Dy, is unable to induce a ferromagnetic transition. On the other hand, the hexagonal crystal-field anisotropy is nearly three times as big as in Dy, and distorts the helix drastically when the temperature is reduced, as revealed by the appear-

ance of higher harmonics in neutron diffraction (Koehler *et al.* 1966). As illustrated in Fig. 2.4, the peak in $\mathcal{J}(\mathbf{q})$ simultaneously moves to smaller values of $\mathbf{q}$, and the $\mathbf{Q}$ of the magnetic structure decreases correspondingly. However this change does not occur uniformly with temperature, but rather a series of *commensurable* wave-vectors is traversed, with apparently discontinuous jumps between them (Gibbs *et al.* 1985). At 20 K, a second-order transition to a shallow cone structure, with an opening angle which decreases continuously towards 80° as the temperature is lowered, is observed. The helical component is commensurable with the lattice, with an average turn angle of 30°, but the moments are strongly bunched around the easy b-axes, as shown in Fig. 1.20.

To interpret this rich variety of phenomena, we will use the model of Larsen *et al.* (1987). The Hamiltonian which they constructed has

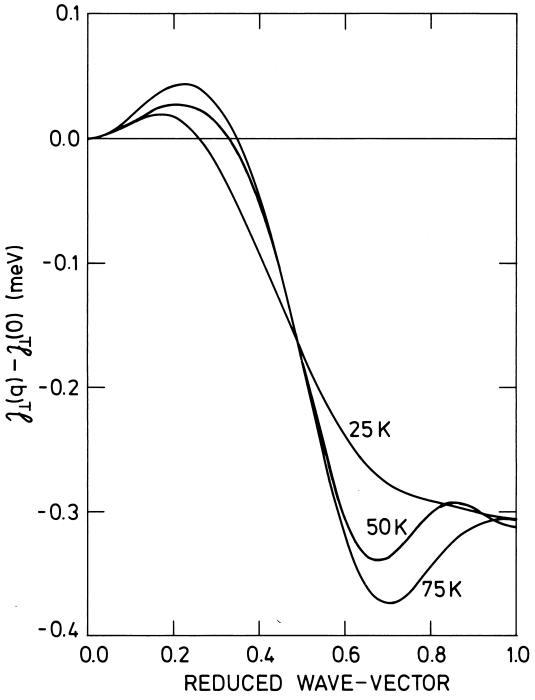

Fig. 2.4. The Fourier transform, for wave-vectors in the c-direction, of the indirect-exchange interaction in Ho at different temperatures, deduced from the magnetic excitations and used in the calculation of the structures. The maximum in $\mathcal{J}_\perp(\mathbf{q})$ increases in magnitude and moves to larger wave-vectors as the temperature is increased, leading to a decrease in the repeat distance of the periodic structures.

the form of (2.1.1), augmented by the magnetic dipole–dipole interaction (1.4.26) which, as we shall see, is of crucial importance. The crystal-field parameters B_l^m were determined primarily from a fit to the magnetic structures and magnetization curves at low temperatures, shown in Fig. 1.20, and the temperature dependence of these parameters was assumed to be negligible. The initial values for the isotropic Heisenberg exchange were taken from an analysis of the spin waves in Ho (Jensen 1988a), and depend explicitly on the temperature, as shown in Fig. 2.4. They were adjusted slightly (Mackintosh and Jensen 1990) to reproduce correctly the transition fields from the helical phase, but remain consistent with the spin-wave data, within the experimental error. The magnetic properties are calculated by means of the method described in Section 2.1.2, assuming an initial distribution $\langle \mathbf{J}_i \rangle$ of the moments at a given temperature. The structure is taken to be commensurable, with a repeat distance, deduced from experimental data, which may be as high as 50–100 atomic layers for the more complex configurations. The assumed values of $\langle \mathbf{J}_i \rangle$ are inserted into the Hamiltonian and a new set of moments calculated, using the mean-field method to reduce the two-ion term to the single-ion form. This procedure is repeated until self-consistency is attained. The free energy and the moments on the different sites can then readily be calculated for the self-consistent structure.

The results of such self-consistent calculations for different temperatures and commensurable periodicities are shown in Fig. 2.5. The data indicate that B_4^0 is zero, to within the experimental error, whereas B_6^0 has the opposite sign to B_2^0. As the temperature is reduced in the helical phase and $B_6^0\langle O_6^0\rangle$ increases, this term tends to pull the moments out of the plane. If the only two-ion coupling were the isotropic exchange, this would give rise to a continuous transition to a tilted helix, which reduces the exchange energy more effectively than the cone (Elliott 1971, Sherrington 1972). However, the dipolar interaction strongly favours a ferromagnetic orientation of the c-axis moments, because the dipolar energy associated with a longitudinal wave is very high, as we discuss in detail in Section 5.5.1. Consequently, the dipolar contribution shifts the position of the maximum in $\mathcal{J}_\parallel(\mathbf{q})$ from $\mathbf{q} = \mathbf{Q}$ to zero wave-vector, as illustrated in Fig. 5.7, and the vanishing of the axial anisotropy (2.2.33) at $\mathbf{q} = \mathbf{0}$ leads to a second-order transition at T_N' to the cone phase. In this special case, we can therefore conclude that it is the temperature dependence of $B_6^0\langle O_6^0\rangle$ which drives the helix into instability, and that the dipolar interaction chooses the cone, rather than the tilted helix, as the stable low-temperature phase.

At 4 K, in the cone phase, the large hexagonal anisotropy causes the helical component of the moments to bunch around the easy directions of magnetization, in the twelve-layer structure described by eqn (1.5.3),

so that the constant angle ϕ in the plane between any moment and the nearest b-axis is only 5.8°, as shown in Fig. 2.5(a), compared with the 15° which corresponds to a uniform helix. As the temperature is increased, the expectation value $\langle O_6^6 \rangle$ decreases with the relative magnetization, roughly like σ^{21}, and ϕ increases correspondingly. Simultaneously $\mathbf{Q}$ tends to increase, reflecting the change in the position of the maximum

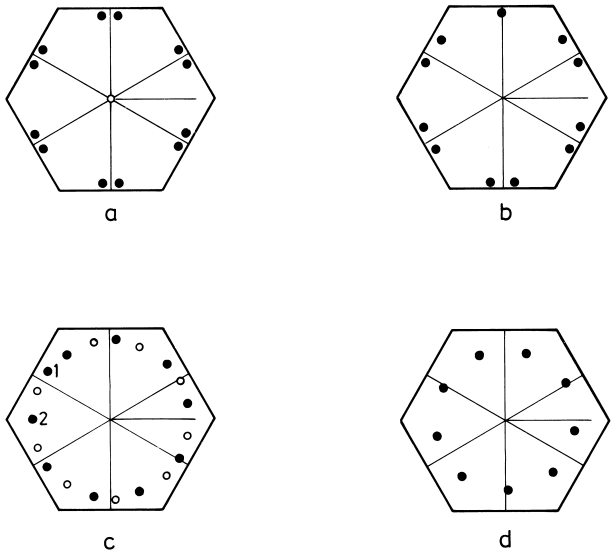

Fig. 2.5. The self-consistent periodic structures in Ho, calculated at different temperatures. Each circle represents the magnitude and direction of the ordered moment in a specific plane, relative to the size of the moment at absolute zero ($10\,\mu_B$), indicated by the length of the horizontal lines. The orientation of moments in adjacent planes is depicted by the positions of neighbouring circles.

(a) The 12-layer zero-spin-slip structure at 4 K. The open circle in the centre indicates the ferromagnetic component in the cone structure.

(b) The 11-layer one-spin-slip structure at 25 K. The bunched pairs of moments are disposed unsymmetrically with respect to the easy axis in the vicinity of the spin slip.

(c) The 19-layer structure at 50 K. The orientation of the moments in successive layers is determined by following first the filled circles in an anticlockwise direction, as indicated, and then the open circles.

(d) The 9-layer trigonal structure at 75 K. This may be looked upon as a three-spin-slip structure, but the bunching is so slight that it is more useful to regard it as an almost regular helix, in which every third plane aligns its moments close to an easy axis, in order to reduce the anisotropy energy.

in $\mathcal{J}(\mathbf{q})$, so that the structure at 25 K has reduced its periodicity to 11 layers by introducing a regularly-spaced series of *spin slips*, at which one plane of a bunched doublet is omitted while the remaining member orients its moments along the adjacent easy axis. The configuration of Fig. 2.5(b), in which one spin slip is introduced for each repeat distance of the perfect commensurable structure, is the primordial spin-slip structure and has a number of interesting features. It is particularly stable, existing over a range of temperature (Gibbs *et al.* 1985), possesses a net moment, and the bunching angle is still rather small. Although the angle 2ϕ between two bunched planes is almost constant, the exchange interaction distorts the structure near the spin slips so that the moments are not symmetrically disposed around the easy axis. As the temperature is increased further, the bunching decreases and the concept of spin slips becomes less useful. Thus the configuration of Fig. 2.5(d) can be considered as a distorted three spin-slip structure, but it is simpler to regard it as a commensurable, almost regular helix in which every third plane aligns its moments close to an easy axis in order to reduce the anisotropy energy.

The spin-slip structures of Ho have been subjected to a careful and extensive neutron-diffraction study by Cowley and Bates (1988). They interpreted their results in terms of three parameters:

b - the number of lattice planes between spin slips,

2α - the average angle between the moments in a bunched pair,

σ_G - a Gaussian-broadening parameter for α.

In a perfect, undistorted structure, $\alpha = \phi$ and $\sigma_G = 0$. The parameter σ_G takes into account two effects; the distortions which occur in perfect periodic structures such as that illustrated in Fig. 2.5(b), and possible irregularities in the positions of the spin-slip planes. The former is in principle included in the calculations, whereas the latter is not. From the calculated magnetic structures, such as those illustrated in Fig. 2.5, it is possible to deduce the corresponding neutron-diffraction patterns and hence, by fitting the peak intensities, determine the values for α and σ_G (Mackintosh and Jensen 1990). The parametrization suggested by Cowley and Bates is in practice rather satisfactory; it allows a fit of all the calculated neutron-diffraction intensities, which vary over about five orders of magnitude, with a relative error of in all cases of less than 20%. Furthermore, the parameter α is close to the average values of the angle ϕ determined directly from the calculated structures. The measured and calculated values of α are in good agreement, taking into account the experimental uncertainties, but there are some discrepancies in σ_G. It is noteworthy that the agreement between the predicted and observed neutron-diffraction intensities is very good for the $b = 11$, one-spin-slip structure, but that the experimental values of σ_G otherwise

lie consistently above the theoretical. This may indicate that the perfect periodicity of the less stable spin-slip structures is more effectively disturbed by imperfections.

As may be seen from Table 2.1, the easy direction in Er is the c-axis at high temperature, so the moments order in a longitudinal-wave structure at T_N. As the temperature is reduced, the structure squares up, as discussed in Section 2.1.4. The basic wave-vector $\mathbf{Q}$ describing the magnetic ordering increases approximately linearly just below T_N (Atoji 1974; Habenschuss *et al.* 1974). This is not in accord with the quadratic dependence predicted by (2.1.35*b*) and furthermore, since $\mathcal{J}'(3\mathbf{Q})$ is probably negative, the predicted change in $\mathbf{Q}$ also has the opposite sign to that observed. This behaviour can only be accounted for if $\mathcal{J}(\mathbf{q})$ is temperature dependent, as is indicated even more clearly at lower temperatures, where $\mathbf{Q}$ starts to decrease quite rapidly. At $T_N' \simeq 52\,\mathrm{K}$, a basal-plane component begins to order, through the mechanism described in Section 2.1.5. When the temperature is lowered further, $\mathbf{Q}$ continues to decrease, exhibiting a number of plateaux, and a rich harmonic structure is observed (Atoji 1974; Habenschuss *et al.* 1974; Gibbs *et al.* 1986). Very detailed neutron-diffraction measurements by Cowley (1991) have revealed a whole sequence of commensurable structures with decreasing temperature, with $Q = 2/7$, $3/11$, $7/26$, $4/15$, $5/19$, $6/23$, and $1/4$, in units of $2\pi/c$. At 18 K, a first-order transition to a steep cone, with an opening angle of 30° and a wave-vector of $\sim 5/21$, is observed.

To explain these results, we may employ a modified version of the model of Jensen (1976b), in which crystal fields, isotropic exchange, and dipolar interactions are included. In addition, the anisotropic two-ion coupling, which is required by the observed excitation spectrum and discussed in Section 6.1, is also taken into account. Mean-field calculations then predict that the structure in the intermediate temperature range is an elliptic cycloid, the hodograph of which at 48 K, just below the transition temperature, is shown in Fig. 2.6. As discussed in Section 2.1.5, an additional second-order transition may occur below T_N', to a phase with a non-collinear, elliptical ordering of the basal-plane moments. In the presence of random domains, the neutron-diffraction patterns from the two structures are essentially indistinguishable, and if this transition occurs in Er, the fluctuations expected near a second-order transition may also be suppressed, because it is then likely that it coincides with one of the first-order commensurable transitions. The model calculations indicate that the non-collinear component in the basal plane is close to becoming stable when the cycloidal phase is disrupted by the first-order transition to the cone phase. Hence it is most probable that the moments in Er are ordered in a planar elliptic-cycloidal structure in the

whole interval between T_C and T'_N, but it is possible that a non-collinear basal-plane component is present in some of the commensurable structures just above T_C.

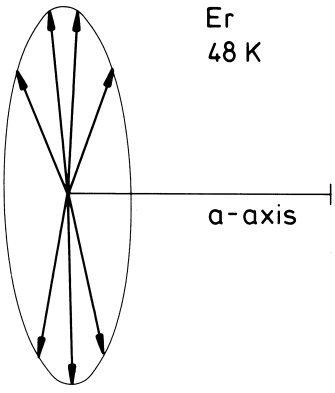

Fig. 2.6. The calculated magnetic structure in Er at 48 K. Each arrow represents the magnitude and orientation, in the a-c plane, of the ordered moment in a specific plane normal to the c-axis, relative to the magnitude of the moment at absolute zero ($9\,\mu_B$), indicated by the length of the line along the a-axis. The hodograph is very close to an ellipse, with semi-axes of length 6.5 and $2.2\,\mu_B$, and this structure can be considered as comprising four planes of moments with a positive component along the c-axis, followed by three with a negative moment, with the designation (43).

The structure shown in Fig. 2.6 comprises four planes of moments with a positive component along the c-axis, followed by three with a negative moment. The basic wave-vector is therefore 2/7, and we may describe the structure as (43). The other commensurable structures listed above are then respectively 2×(443), 2×(4434443), (4443), 2×(44443), (444443), and (44) where, in each case, blocks of n moments with a positive component along the c-axis alternate with negative blocks, and the doubling is necessary to ensure periodicity if the number of blocks is odd. These calculations give a good account of the neutron-diffraction results of Cowley (1991). The lattice strains associated with a number of these structures have been studied with synchrotron X-rays by Gibbs *et al.* (1986). The fundamental wave-vector for the oscillating c-axis strain in a structure like (44), which has inversion symmetry, is twice that of the magnetic structure. However, the other examples above do not have inversion symmetry, so charge-scattering of X-rays may occur at the fundamental magnetic wave-vector. In the cone phase, the X-ray scattering at the fundamental wave-vector of the helical component is anomalously large, even though the longitudinal lattice-strain must be very small. There is however also a contribution from charge scattering associated with a *transverse* strain, discussed at the end of the previous section, which may arise when the mirror symmetry normal to the c-axis is broken, as it is in this structure. The hexagonal symmetry of a

particular plane is then maintained, but it suffers a lateral displacement which follows the direction of the helical component of the moment.

The transition from the cycloidal to the cone structure in Er at 18 K reflects a shift in the balance between a number of competing effects. At this low temperature, the entropy is not important, since most of the moments are close to their saturation value near T_C, nor does the difference between the single-ion crystal-field anisotropy energy in the two phases play a significant role. Because of cancellation among the three contributions, the axial anisotropy is relatively insensitive to the angle between the c-axis and the moments, the average value of which does not, in any case, change much at the transition. The small amplitude of the basal-plane components ensures that the hexagonal-anisotropy energy also has only a minor influence. Hence the choice between the two phases is dominated by the two-ion contributions to the energy. From the spin-wave dispersion relation, discussed in Section 6.1, the difference $\mathcal{J}_\perp(\mathbf{Q}) - \mathcal{J}_\perp(\mathbf{0})$ is estimated to be about 0.07–0.1 meV, strongly favouring a modulated structure. The tendency towards a modulation of the c-axis component is opposed by three effects. Firstly, the anisotropy of the classical dipole–dipole contribution reduces $\mathcal{J}_\parallel(\mathbf{Q}) - \mathcal{J}_\parallel(\mathbf{0})$ by 0.03 meV to about 0.04–0.07 meV. Secondly, the modulated ordering of the c-axis component cannot take full advantage of the large value of $\mathcal{J}_\parallel(\mathbf{Q})$, because of the squaring up which occurs as the temperature is decreased. The energy due to the coupling of the longitudinal component of the moments is

$$U_{\zeta\zeta} = -\tfrac{1}{4}N \sum_{n\ \mathrm{odd}} \mathcal{J}_\parallel(n\mathbf{Q})\langle J_\zeta(n\mathbf{Q})\rangle^2 = -\tfrac{1}{2}N\overline{\mathcal{J}}_\parallel(\mathbf{Q})\langle|J_\zeta|\rangle^2, \quad (2.3.1a)$$

introducing the effective coupling parameter $\overline{\mathcal{J}}_\parallel(\mathbf{Q})$. At high temperatures, close to T_N, the two coupling parameters $\overline{\mathcal{J}}_\parallel(\mathbf{Q})$ and $\mathcal{J}_\parallel(\mathbf{Q})$ are equal, but as the higher odd harmonics gradually develop, $\overline{\mathcal{J}}_\parallel(\mathbf{Q})$ decreases, and when the structure is close to the square wave, we find from (2.1.36) that

$$\overline{\mathcal{J}}_\parallel(\mathbf{Q}) \simeq \frac{8}{\pi^2}\{\mathcal{J}_\parallel(\mathbf{Q}) + \tfrac{1}{9}\mathcal{J}_\parallel(3\mathbf{Q}) + \cdots\}. \quad (2.3.1b)$$

Just above the cone transition, the model calculations indicate that $\overline{\mathcal{J}}_\parallel(\mathbf{Q})$ is reduced by 0.02–0.03 meV, compared to $\mathcal{J}_\parallel(\mathbf{Q})$, which in combination with the dipolar term removes most of the energy difference between the modulated and ferromagnetic ordering of the c-axis component. The final contribution, which tips the balance into the cone phase below T_C, is the magnetoelastic energy associated with the α-strains

$$U^\alpha_{\mathrm{me}} = -\tfrac{1}{2}(c_{11} - c_{66})(\epsilon_{11} + \epsilon_{22})^2 - \tfrac{1}{2}c_{33}\epsilon_{33}^2 - c_{13}(\epsilon_{11} + \epsilon_{22})\epsilon_{33}. \quad (2.3.2)$$

The abrupt change in the uniform α-strains (Rhyne and Legvold 1965b) at the transition to the cone phase reduces this energy by 0.19 meV/ion (Rosen *et al.* 1973), corresponding to an increase of $\mathcal{J}(\mathbf{0})$ by about 0.01 meV. In the cycloidal phase, there is also a longitudinal-strain mode at wave-vector $2\mathbf{Q}$, which disappears in the cone phase, but the energy gained by this distortion is estimated to be very small. Since the c-axis moment is substantially squared up in the cycloidal phase just above the transition, the change of the α-strains cannot have its origin in the single-ion magnetoelastic coupling, which does not distinguish between positive and negative moments. It must rather be caused by the strain-dependence of the two-ion interaction

$$\Delta\mathcal{H}_{\rm me} = -\sum_{ij}\big[I_1(ij)\{\epsilon_{11}(i)+\epsilon_{22}(i)\}+I_3(ij)\epsilon_{33}(i)\big]J_{i\zeta}J_{j\zeta}, \quad (2.3.3)$$

which is that part of eqn (2.2.32) which changes at the transition. If the basal-plane moments and the single-ion magnetoelastic terms are assumed to be the same immediately above and below T_C, $\Delta\mathcal{H}_{\rm me}$ gives rise to the following changes at the transition:

$$\begin{aligned}(c_{11}-c_{66})\Delta(\epsilon_{11}+\epsilon_{22})+c_{13}\Delta\epsilon_{33} &= N\{I_1(\mathbf{0})-\overline{I}_1(\mathbf{Q})\}\langle|J_\zeta|\rangle^2\\ c_{13}\Delta(\epsilon_{11}+\epsilon_{22})+c_{33}\Delta\epsilon_{33} &= N\{I_3(\mathbf{0})-\overline{I}_3(\mathbf{Q})\}\langle|J_\zeta|\rangle^2,\end{aligned} \quad (2.3.4)$$

where the bars denote effective coupling parameters, as in (2.3.1), and $\Delta\epsilon_{\alpha\alpha}=\epsilon_{\alpha\alpha}(\text{cone})-\epsilon_{\alpha\alpha}(\text{cycloid})$. Since the elastic constants are known, and the strains are $\Delta\epsilon_{33}=3.1\cdot10^{-3}$ and $\Delta(\epsilon_{11}+\epsilon_{22})=-2.4\cdot10^{-3}$, the two-ion magnetoelastic-coupling parameters may be determined from this equation. The nature of this magnetoelastic contribution implies that it should be possible to suppress the cone phase in Er by applying hydrostatic pressure. In the zero-temperature limit, the energy difference between the two phases is estimated to be only about 0.033 meV/ion, so a hydrostatic pressure of about 2.5 kbar, or alternatively a uniaxial pressure along the c-axis of only about half this amount, should be sufficient to quench the cone. The application of this modest pressure should then allow experimental studies of the cycloidal phase in Er below 18 K, to ascertain, for example, whether the transition to the phase with an elliptical ordering of the basal-plane moments occurs. We shall return to this two-ion magnetoelastic interaction when we discuss Er films and superlattices.

The negative value of B_2^0 in Tm is large and B_6^0 is also negative, as may be seen in Table 2.1, so that the moments are firmly anchored to the c-direction, and no ordered basal-plane component appears at any temperature. A longitudinal-wave structure forms at 56 K, and starts to square up at about 40 K, as the amplitude approaches the free-ion

moment of $7.0\,\mu_B$. At 32 K, there is a first-order transition to a commensurable state, with a seven-layer repeat distance, which has a ferromagnetic component (Brun *et al.* 1970). At the lowest temperatures, this has developed into a *ferrimagnetic* square-wave structure, comprising a repeating pattern of four layers of positive moments followed by three of negative moments. These structures, the susceptibility curves of Fig. 2.1, and the excitation spectrum have been used to determine the parameters of a model for Tm with the usual basic ingredients of isotropic exchange, crystal fields, and dipolar interactions (McEwen *et al.* 1991). As shown in Fig. 2.7, the observed squaring-up process is very well accounted for by mean-field calculations based on this model. The principal discrepancy with experiment is in the magnitude of the field along the c-axis which is required to form a ferromagnetic structure, where the calculation gives a value about 50% above the observed 28 kOe. This may indicate that the form of $\mathcal{J}(\mathbf{q})$ in Tm which, as illustrated in Fig. 1.17, has the largest peak in the whole heavy rare earth series, changes substantially at this first-order transition.

The magnetic structures of the light rare earths have not generally been described in the same detail as those of the hcp metals, with the exception of Nd, which has been intensively studied for several decades.

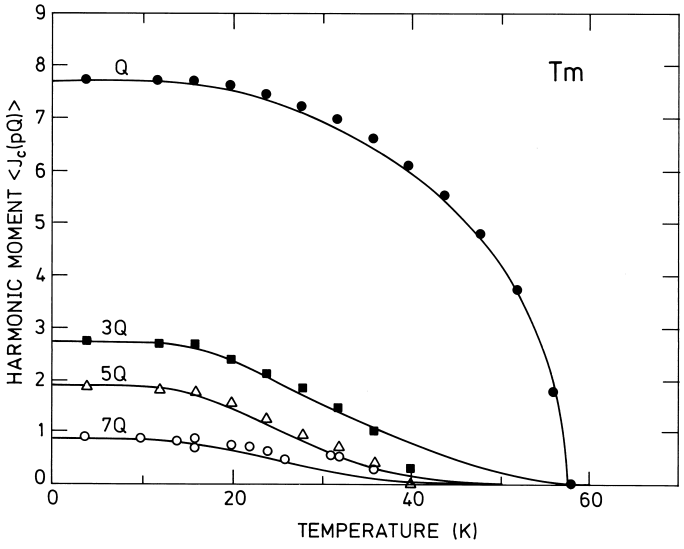

Fig. 2.7. The calculated harmonics of the c-axis moment in Tm as a function of temperature, compared with the results of neutron diffraction measurements, and the ferromagnetic moment ($7Q$).

Such is the complexity of the observed neutron diffraction patterns, however, that it is only recently that a reasonably complete delineation of the ordered moments has been attained (Zochowski *et al.* 1991). At the Néel temperature of 19.9 K, a weakly first-order transition leads to a longitudinal-wave structure propagating in a b-direction on the hexagonal sites of the dhcp structure, with an incommensurable periodicity given by $\mathbf{Q}_h = 0.13\mathbf{b}_1$. The moments on neighbouring hexagonal layers are ordered antiferromagnetically. Simultaneously, a c-axis moment (plus a small component in the basal plane) with the same $\mathbf{Q}$ is induced on the cubic sites by the anisotropic two-ion coupling. The moments on neighbouring cubic layers are also ordered antiferromagnetically. As the temperature is further lowered, another first-order transition at 19.2 K establishes a double-$\mathbf{Q}$ structure, with wave-vectors $\mathbf{Q}_1$ and $\mathbf{Q}_2$ aligned approximately along a pair of b-axes but canted slightly, so that the angle between them is somewhat less than 120°. The polarization vectors of the moments in the two waves are also canted away from the corresponding b-axes and towards each other, but by a different amount from the wave-vectors, so that the waves are no longer purely longitudinal. Compared with the single-$\mathbf{Q}$ structure, this arrangement increases the average ordered moment, which is further augmented, as the temperature is lowered, by a squaring-up of the structure, which generates harmonics in the neutron-diffraction pattern. Simultaneously, the period gradually increases. At 8.2 K, the planar components of the moments on the cubic sites begin to order, and after undergoing a number of phase transitions, the structure at low temperatures is characterized by the four $\mathbf{Q}$-vectors illustrated in Fig. 2.8. Although all four periodicities are present on each type of site, $\mathbf{Q}_1$ and $\mathbf{Q}_2$, which are now aligned precisely along b-axes, but have different magnitudes $0.106b_1$ and $0.116b_1$, generate the dominant structures on the hexagonal sites, while $\mathbf{Q}_3$ and $\mathbf{Q}_4$, which have lengths $0.181b_1$ and $0.184b_1$ and are canted towards each other, predominate on the cubic sites. The different types of $\mathbf{Q}$-vector are interrelated; within the experimental uncertainty $\mathbf{Q}_3 + \mathbf{Q}_4 = 2\mathbf{Q}_1$, and the canting of $\mathbf{Q}_3$ and $\mathbf{Q}_4$ is related to the difference in length between $\mathbf{Q}_1$ and $\mathbf{Q}_2$.

The explanation of these structures from first principles in terms of the elementary magnetic interactions is clearly a formidable task but, as we have seen in Section 2.1.6, the ordering on the hexagonal sites at high temperatures can be satisfactorily accounted for by a phenomenological Landau expansion of the free energy in terms of the order parameters, and the role of the different interactions thereby clarified. The anisotropic two-ion coupling between the dipoles confines the moments to the basal plane and tends to favour the longitudinal-wave structure. Two-ion coupling between the quadrupoles, proba-

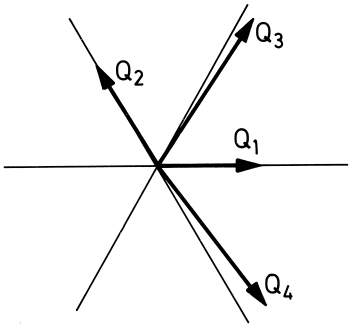

Fig. 2.8. The relative orientations and magnitudes of the fundamental wave-vectors which describe the quadruple-**Q** magnetic structure of Nd at low temperatures. All four periodicities are present on each type of site, but $\mathbf{Q}_1$ and $\mathbf{Q}_2$ generate the dominant structures on the hexagonal sites, while $\mathbf{Q}_3$ and $\mathbf{Q}_4$ predominate on the cubic sites.

bly of magnetoelastic origin, lifts the degeneracy between the different multiple-**Q** structures and stabilizes the single-**Q** state just below T_N. The Landau expansion can also explain the rotation of the wave-vectors and moments away from the *b*-axes, with the consequent stabilization of the double-**Q** configuration, and account for the observed harmonics in this structure. A similar analysis for the quadruple-**Q** structure in the low-temperature region would provide the basis for understanding the even more complicated phenomena which are observed when a magnetic field is applied to Nd (Zochowski *et al.* 1991).

2.3.2 The magnetization of Holmium

The analytical mean-field treatment by Nagamiya *et al.* (1962) of the effect of a magnetic field applied in the plane of a helical structure was mentioned in Section 1.5. As the field is increased, the helix first distorts, giving rise to a moment along **H**, and then undergoes a first-order transition to a fan structure, in which the moments oscillate about the field direction. A further increase in the field reduces the opening angle of the fan which, in the absence of magnetic anisotropy, goes continuously to zero, establishing a ferromagnetic phase at a second-order transition. Hexagonal anisotropy may modify this process by inducing a first-order transition or, if it is large enough, eliminate the fan phase entirely.

The magnetization curves measured by Strandburg *et al.* (1962) and Féron (1969) behaved in accordance with this description at low temperatures, but above about 40 K when the fan phase was first observed, a further phase also appeared, manifested by a plateau corresponding to a moment about one half of that attained in the fan phase. This extra phase was clearly apparent in the magnetoresistance measurements of Mackintosh and Spanel (1964), and later experiments by Akhavan and Blackstead (1976), in which the field was changed continuously, revealed

as many as five different phases at some temperatures. The structures in a magnetic field were investigated with neutron diffraction by Koehler *et al.* (1967), who identified two intermediate phases which they called fans and characterized by the intensity distribution of the Bragg peaks.

These phenomena have been elucidated by means of calculations of the effect of a magnetic field on the commensurable structures of Fig. 2.5 (Jensen and Mackintosh 1990). At low temperatures, the hexagonal anisotropy has a decisive influence on the magnetic structures, ensuring that a first-order transition occurs from the helix or cone to the ferromagnet, without any intermediate phases. Below about 20 K, where the cone is the stable structure in zero field, the cone angle is almost independent of the applied field in the basal plane, but at the transition to the ferromagnet, the c-axis moment disappears. When the field is applied in the hard direction at these temperatures, the moments just above the ferromagnetic transition do not point along the field direction, but are aligned very closely with the nearest easy axis, so that $\langle J_{\parallel} \rangle \simeq 8 \cdot \sqrt{3}/2$, as illustrated in Fig. 1.20. As the field is further increased, they turn towards it, becoming fully aligned through a second-order phase transition at a critical field which is estimated from B_6^6 to be about 460 kOe at absolute zero. At low temperatures, the hexagonal anisotropy also hinders the smooth distortion of the helix in a field. The moments jump discontinuously past the hard directions as the field is increased, giving first-order transitions which may have been observed, for example, as low-field phase boundaries below 20 K in the measurements of Akhavan and Blackstead (1976).

Above about 40 K, when the hexagonal anisotropy is not so dominant, intermediate stable phases appear between the helix and the ferromagnet. The nature of these phases may be appreciated by noting that the helix can be considered as blocks of moments with components alternately parallel and antiparallel to the field, as is apparent from the structures illustrated in Fig. 2.5. If we write this pattern schematically as $(+\,-\,+\,-)$, then the fan structure may be described as $(+\,+\,+\,+)$. The intermediate structures, the helifans, then correspond to patterns of the type specified in Table 2.2. The notation helifan(p) is used to designate a structure whose fundamental period is p times that of the helix (the single number p is not generally adequate for discriminating between the different helifans). It is clear that these structures represent compromises between the demands of the exchange for a periodic structure, and the field for a complete alignment of the moments. They are not due to the hexagonal anisotropy which, on the contrary, tends to suppress them, and occur both when the field is applied along the easy and hard directions in the plane. The free energies of the various magnetic phases as a function of magnetic field in the easy direction at

Table 2.2. The arrangement of blocks of spins in the helifan structures. The first row shows the relative number of (−) blocks in the different structures.

	Helifan				
Helix	(4)	(3)	(3/2)	(2)	Fan
1/2	3/8	1/3	1/3	1/4	0
+	+	+	+	+	+
−	+	+	+	+	+
+	+	+	−	+	+
−	−	−	+	−	+
+	+	+	+	+	+
−	−	−	−	+	+
+	+	+	+	+	+
−	−	+	+	−	+
+	+	+	−	+	+
−	+	−	+	+	+
+	+	+	+	+	+
−	−	−	−	−	+

50 K are shown in Fig. 2.9. In these calculations, the wave-vector **Q** was allowed to vary in small, discrete steps, by changing the repeat distance, and the absolute minimum in the free energy for the structure thereby determined, as illustrated in the insert to Fig. 2.9, leading to the prediction that the stable magnetic structures follow the sequence helix → helifan(3/2) → fan → ferromagnet as the field is increased. The helifan(3/2) is depicted in Fig. 2.10. In a narrow interval between the helix and the helifan(3/2), other stable phases appear, e.g. the helifan(4′) (+ + − + + − + −), and similarly a sequence of helifans with m (+) blocks followed by a (−) ($m \geq 3$) occurs in the close neighbourhood of the fan phase. The various structures are associated with characteristic neutron-diffraction patterns. An examination of the neutron-diffraction intensities which Koehler *et al.* (1967) associate with the phase which they designate as 'Fan I' reveals a striking correspondence with the helifan(3/2) pattern, with a very weak fundamental at $\mathbf{Q}_0/3$, where $\mathbf{Q}_0$ is approximately the wave-vector of the helix, strong second and third harmonics, and a weak fourth harmonic. The basic periodicities of this structure are $2\mathbf{Q}_0/3$ for the component of the moments parallel to the field, and $\mathbf{Q}_0$ for the perpendicular component; the weak $\mathbf{Q}_0/3$ peak arises as the result of interference between them. Similar but more detailed neutron-diffraction results have more recently been obtained by Axe *et al.* (1991). The changes in the basic wave-vector are substantial,

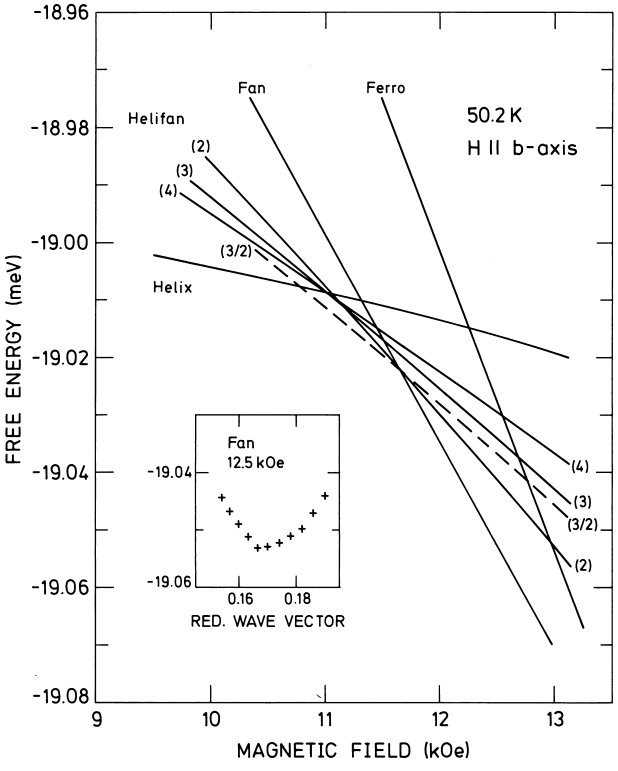

Fig. 2.9. Mean-field calculation of the free energy per ion for different magnetic structures in Ho at 50 K, as a function of the magnetic field along an easy b-axis. The free energy is in each case minimized with respect to the wave-vector which characterizes the structure, as illustrated for the fan phase in the insert.

even though the underlying exchange function is constant, and they agree very well with those observed by neutron diffraction. For the helix, fan and helifan(3/2) structures, the experimental (theoretical) values of Q are respectively 0.208 (0.211), 0.170 (0.168), and 0.063 (0.066), times $2\pi/c$. The period of the fan phase increases relative to that of the helix because of the resulting increase in the opening angle of the fan, expressed by the relation (1.5.21). This allows a decrease in the exchange energy which is greater than the concomitant increase of the Zeeman energy. The change in $\mathbf{Q}$ in the various helifan phases is therefore to a very good approximation proportional to their magnetization.

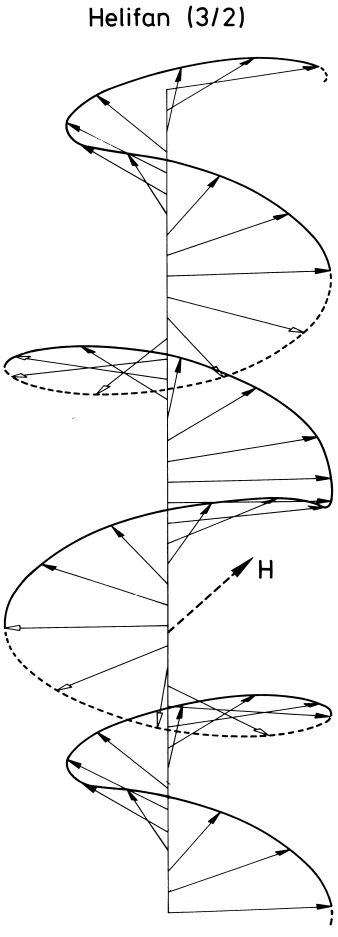

Fig. 2.10. The helifan(3/2) structure in Ho at 50 K. The moments lie in planes normal to the *c*-axis and their relative orientations are indicated by arrows. A magnetic field of 11 kOe is applied in the basal plane, and moments with components respectively parallel and antiparallel to the field are designated by filled and open arrow-heads. This component of the moments has a periodicity which is 3/2 that of the corresponding helix, and the helicity of the structure changes regularly.

A detailed consideration (Mackintosh and Jensen 1990) of the magnetization curves measured in Ho indicates that the metastable helifan(2) may replace or co-exist with the stable (3/2)-structure, if the measurements are made so rapidly that complete thermodynamic equilibrium is not attained. Other stable or metastable helifans may be involved in the five phases observed by Akhavan and Blackstead (1976). In addition, the very pronounced hysteresis which they observed is consistent with the existence of a large number of phases which have almost the same energy, but are not easily transformed into each other.

The stability of the various periodic structures is determined by the form of the two-ion coupling, especially the long-range component. If

the exchange is sufficiently short-range, the helix, helifans and fan are almost degenerate at the critical field; it is the interaction between the blocks which differentiates between these structures. One of the most remarkable features of the helifans is the large number of hexagonal layers involved in a single period, a characteristic which they share with the commensurable structures observed in zero field in Ho and Er, which were discussed in the preceding sub-section.

Helifans, or analogous structures, may also occur in other rare earth systems where periodic ordering is observed. For example, the modulated structures in Nd discussed previously may be described as $(+-+-+-+-)$, indicating blocks of moments with a component parallel or antiparallel to a magnetic field applied in the basal plane. A periodic reversal of $(-)$ blocks will then generate subharmonics of the basic $\mathbf{Q}$-vector. Thus the sequence $(+++-+-+-)$ generates $\mathbf{Q}/4$, and $(+++-+++-)$ gives $\mathbf{Q}/2$, both of which have been observed by neutron diffraction in a magnetic field (Zochowski *et al.* 1991).

2.3.3 Films and superlattices

The development of the technique of *molecular-beam epitaxy* has allowed the fabrication on a substrate of films of rare earth metals, with thicknesses ranging from a few to thousands of atomic planes. In addition, *superlattices*, or *multilayers*, of the form $[A_l|B_m]_n$ may be produced, in which blocks comprising l planes of element A, followed by m planes of element B, are replicated n times. It is clear that an endless variety of such systems may be constructed, and the field is in a stage of rapid development. We will restrict ourselves to a discussion of some of the new physical principles involved in understanding the magnetic properties of such structures, illustrated by a few specific examples.

The essential difference between these structures and a bulk crystal lies, of course, in the boundary conditions. Films and superlattices are *finite* in one dimension, whereas a bulk crystal is assumed to be essentially unbounded, and the magnetic layers are terminated by a medium which may have very different magnetic properties, be it a vacuum, a rare earth with quite different moments and interactions, or a nominally non-magnetic metal such as Y, which is a very popular choice for the intermediate layers in superlattices.

The influence of the finite size on the orientation of the ordered moments is illustrated in Fig. 2.11, which depicts the results of a mean-field calculation, based on the model of Larsen *et al.* (1987), for a 15-plane slab of Ho at 4 K. The bunched commensurable helix encompassing the inner 12 planes is enclosed by a single and a double plane, aligned almost ferromagnetically with the respective outer planes. These ferromagnetic clusters distort the adjacent bunched pairs in a manner reminiscent of

spin slips. Such ferromagnetic terminations at the surfaces of slabs containing planes of rotating moments are a general feature, reflecting the predominantly ferromagnetic interaction between closely neighbouring planes in the magnetic rare earths. This coupling normally gives rise to a net moment in the slab, and is calculated to stabilize ferromagnetic ordering at 4 K in samples thinner than about nine atomic planes (Bohr *et al.* 1989).

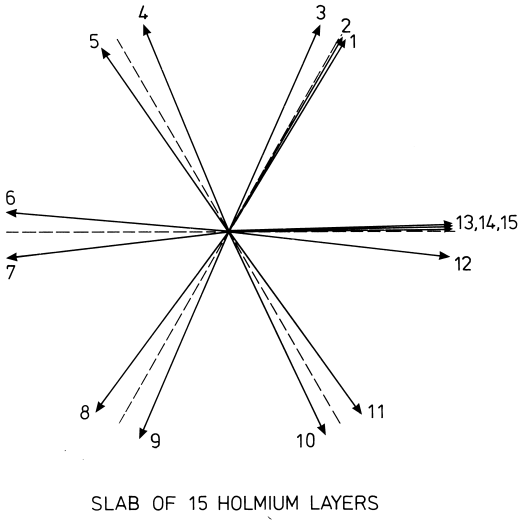

Fig. 2.11. Mean-field calculation of the orientation of the magnetic moments in a 15-plane slab of Ho at 4 K. The inner planes are close to a bunched commensurable helix, but there is a strong tendency to ferromagnetism near the surfaces.

The effect of the epitaxial strain is strikingly illustrated by the behaviour of thin films and superlattices of Dy and Er grown on Y, in both of which ferromagnetism is suppressed, by somewhat different mechanisms, in favour of periodic magnetic ordering. In 16-plane Dy films embedded in Y in a variety of $[Dy_{16}|Y_m]$ multilayers, with the c-axis normal to the plane of the slab, Rhyne *et al.* (1989) found that the helix persists to the lowest temperatures, and the ferromagnetic state is only induced if a field of the order of 10 kOe is applied in the easy direction. An obvious mechanism for this quenching of ferromagnetism is the constraint which the Y slabs impose on the Dy layers, so that the γ-strains which provide the principal driving force for the transition cannot be fully developed.

The ferromagnetic ordering of the axial moment is also suppressed

in c-axis films and superlattices of Er (Borchers *et al.* 1988), but the explanation in this case is not quite so evident. The dipolar energies are unchanged in the films, nor is it likely that the anisotropy and exchange contributions are decisively different. The strain-dependence of the exchange energy, expressed in eqn (2.3.3), can however provide a mechanism. Y has a planar lattice-constant a of 3.648 Å, which is over two per cent greater than that of Er, and the Y substrate therefore imposes a strain on the Er film, which is measured to be $\epsilon_{11} = \epsilon_{22} \simeq 6\times10^{-3}$. If the atomic volume is assumed to be unchanged in the film, $\epsilon_{33} \simeq -12\times10^{-3}$. The difference in exchange energy between the solid and a thin film may then be found from (2.3.4), and is equivalent to a field of 13 kOe acting on the c-axis moment of about $8\,\mu_B$. The above estimate of ϵ_{33} is probably too great, so this calculation may be considered in reasonably good agreement with the observation that Er films with thicknesses between 860 Å and 9500 Å require fields varying linearly between 8 kOe and 3 kOe to establish a ferromagnetic state at 10 K. It is noteworthy that, since Lu has a significantly smaller basal-plane lattice-constant than Er, the cone structure should be favoured in a c-axis epitaxial film grown on Lu.

Many of the characteristic features of rare earth superlattices are demonstrated by the aforementioned [Dy|Y] systems, which are observed to form helical structures over the whole temperature range of magnetic ordering. When the c-axis is normal to the plane of the film, a coherent magnetic structure may be formed, in which the phase and chirality of the helix are maintained over many bilayers, provided that the slabs of non-magnetic Y are not too thick. The coherence length may be estimated from the widths of the neutron-diffraction peaks, and corresponds to more than 10 bilayers if the Y layers are less than about 10 planes thick. If the thickness is increased to about 35 planes, however, the coherence length, which is inversely proportional to the width of the Y layers, is less than the bilayer thickness, so that the helix in one Dy layer is uncorrelated with that in the next. In the long-range coherent structures, the phase change of the helix across the Dy layers corresponds to a turn angle which varies with temperature and shows a tendency to lock in to 30°, with associated bunching. The phase change across the Y layers, on the other hand, is independent of temperature and the turn angle takes the much larger value of about 50°, which is characteristic of the periodic structures formed by dilute alloys of magnetic rare earths in bulk Y. It therefore appears that the magnetic order is propagated through the Y layers by a spin-density wave, which is incipient in the unperturbed metal, and is associated with the very large susceptibility $\chi(\mathbf{Q})$ of the conduction electrons. The helical ordering in the Dy layers of the c-axis superlattice is disturbed by edge effects of the type illustrated for the Ho film in Fig. 2.11. Consequently, the ordered helical

moment falls below the saturation value of $10\,\mu_B$ at low temperatures, even though the total integrated magnetic scattering corresponds to the fully saturated moment. At higher temperatures, the coupling of the net ferromagnetic moment in a Dy layer to an applied magnetic field breaks the coherence of the helical structure between the layers well before the transition to the true ferromagnetic phase occurs. A *b*-axis superlattice, on the other hand, fails to form a coherent magnetic structure even when the Y layer is as thin as 9 planes, since the static susceptibility at $\mathbf{q} = \mathbf{0}$, which is required to propagate the ferromagnetic coupling between the basal planes of the Dy layers through the Y, is not particularly high. The Dy layers therefore form helical magnetic structures with wave-vectors in the plane of the layers, but no coherence of phase or chirality between the layers.